

Review

Fine nanostructure design of metal chalcogenide conversion-based cathode materials for rechargeable magnesium batteries

Wenxing Miao,¹ Hui Peng,¹ Shuzhen Cui,¹ Jingtian Zeng,¹ Guofu Ma,^{1,*} Lei Zhu,^{2,*} Ziqiang Lei,¹ and Yuxi Xu^{3,*}

SUMMARY

Magnesium-ion batteries (MIBs) a strong candidate to set off the second-generation energy storage boom due to their double charge transfer and dendrite-free advantages. However, the strong coulombic force and the huge diffusion energy barrier between Mg^{2+} and the electrode material have led to need for a cathode material that can enable the rapid and reversible de-insertion of Mg^{2+} . So far, researchers have found that the sulfur-converted cathode materials have a greater application prospect due to the advantages of low price and high specific capacity, etc. Based on these advantages, it is possible to achieve the goal of increasing the magnesium storage capacity and cycling stability by reasonable modification of crystal or morphology. In this review, we focus on the application of a variety of sulfur-converted cathode materials in MIBs in recent years from the perspective of microstructural design, and provide an outlook on current challenges and future development.

INTRODUCTION

With the gradual expansion of industrial scale, non-renewable energy sources have been consumed in large quantities, and human society's demand for energy has become more and more intense.^{1–3} In this context, developing a clean and efficient energy storage system has become a common goal for a large number of scientists.⁴ Among other things, battery technology fills a large number of gaps in the field of energy storage.⁵ Decades of research process has achieved brilliant results, especially lithium-ion batteries (LIBs) due to its high energy density and admissible cycle life make mobile phones, computers, and other portable mobile electronic devices. In particular, the current hot new energy vehicles have been unexpected development speed.^{6–10} Unfortunately, the low lithium reserves and severe dendrite problems seriously hinder the further application of LIBs.^{11–15} In an effort to break through long-dormant battery technology, an emerging metal-ion batteries, magnesium-ion batteries (MIBs) has come to the forefront. Compared to LIBs, magnesium metal anodes have a higher earthly reserve thus greatly reducing the cost of construction.^{16–19} Meanwhile, MIBs show excellent safety due to the non-dendritic (spherical or polyhedral) anode deposition morphology with a high melting point (648°C).^{17,20–22} In terms of energy density, Mg has a low electrode potential (−2.37 vs. Standard Hydrogen Electrode (SHE)) with an excellent volume specific capacity (3833 mAh cm^{−3}). Further, MIBs have a higher theoretical energy density than LIBs due to the two charges of Mg^{2+} during cycling.^{23–25} Based on the previous theoretical foundation, MIBs show unrivalled development prospects, nevertheless the development of MIBs is still relatively slow compared to that of LIBs and is still in the primary development stage. One of the reasons hindering their development is the compatibility of magnesium anode and electrolyte.^{26–28} It is well known that the solid electrolyte interphase (SEI) film formed on the lithium metal electrode in LIBs is electronically insulated and ionically conductive, which can greatly reduce the occurrence of side reactions on the anode. In contrast, the SEI film formed by MIBs in most conventional non-aqueous electrolytes is electrically and ionically insulating at the same time, resulting in the inability of Mg^{2+} to migrate back and forth between the cathode and anode, which results in passivation failure of the Mg metal anode.^{29–31} Although several electrolytes have been developed that can reversibly dissolve Mg, issues such as corrosivity and environmental sensitivity have also hindered the further development of MIBs.³² Apart from that, another more important reason is the scarcity of cathode materials.³³ Mg^{2+} carries two charges on itself and has a larger ionic radius compared to Li^+ , which results in a stronger coulombic interaction with the host and higher diffusion energy barriers during the insertion and de-insertion process of Mg^{2+} , which makes all conventional electrode materials perform poorly in MIBs.^{34–36} In order to be able to find a cathode material with excellent performance and capable of reversibly insertion and de-insertion Mg^{2+} , many scientists have put in a lot of efforts.

In 2000, Aurbuch et al.³⁷ developed a first prototype of MIBs with Mo_6S_8 as the cathode material, $Mg(AlCl_2BuEt)_2$ /Tetrahydrofuran (THF) as the electrolyte, and Mg metal as the anode. The MIBs device possessed a good rate capability (0.1–1 mA cm^{−2}) and a wide operating

¹Key Laboratory of Eco-functional Polymer Materials of the Ministry of Education, Key Laboratory of Polymer Materials of Gansu Province, College of Chemistry and Chemical Engineering, Northwest Normal University, Lanzhou 730070, China

²School of Chemistry and Materials Science, Hubei Key Laboratory of Quality Control of Characteristic Fruits And Vegetables, Hubei Engineering University, Xiaogan, Hubei Province 432000, China

³School of Engineering, Westlake University, Zhejiang 310024, China

*Correspondence: magf@nwnu.edu.cn (G.M.), lei.zhu@hbeu.edu.cn (L.Z.), xuyuxi@westlake.edu.cn (Y.X.)

<https://doi.org/10.1016/j.isci.2024.109811>



temperature (-20°C – 80°C), as well as greater than 2000 depth of charge/discharge cycles with no more than 15% capacity degradation. Unfortunately, Chevrel-phase Mo_6S_8 as a first-generation cathode material only exhibits a low discharge capacity of less than 100 mAh g^{-1} with a low operating voltage (1.1 V vs. Mg^{2+}/Mg), which is still far from our expectation. Nevertheless, the report of this innovative work immediately inspired scientists to take a keen interest in the study of MIBs. This day, researchers have studied the performance of various cathode materials in MIBs, which can be broadly categorized as layered metal oxides (vanadium oxides, molybdenum oxides, etc.), layered transition metal sulfur/selenides (molybdenum-based, titanium-based, tungsten-based), other layered cathodes (MXene), polyanionic compounds (phosphates, silicates), and conversion type cathode materials (manganese oxides, and a large number of transition metal sulfur compounds).^{38–40} Among them, intercalation-type cathode materials and conversion-type cathode materials are the types of cathode materials commonly used in MIBs today.⁴¹ Mg^{2+} in intercalation-type materials mainly achieves energy conversion by reversibly insertion and de-insertion between crystal layers without involving the transformation of the physical phase, so generally this material is more structurally stable during cycling.⁴² However, the large electrostatic interactions between the divalent Mg^{2+} and diffusion channels make Mg^{2+} intercalation kinetics slower, so intercalation-type cathode materials are usually confronted with the problems of low discharge capacity and poor rate performance. Tirado et al.⁴³ synthesized prismatic microrods of h-MoO_3 by a hydrothermal method and obtained only a low capacity of $20\text{--}50\text{ mAh g}^{-1}$ in $0.5\text{ M Mg}(\text{TFSI})_2$ in 1,2-Dimethoxyethane (DME) electrolyte. P. Rhodes and co-workers⁴⁴ prepared a V_2O_5 dry gel by a modified ion-exchange method with NaVO_3 solution, which only obtained a discharge capacity of less than 20 mAh g^{-1} at 10 mA g^{-1} in $0.5\text{ M Mg}(\text{ClO}_4)_2$ in acetonitrile (CH_3CN) electrolyte. The low specific capacity of these electrode materials is still far from meeting our requirements for high-performance MIBs.

Compared with intercalation cathode materials, conversion cathode materials based on multi-step conversion reactions can fully utilize the ultra-high capacity contributed by structural reorganization and chemical bond breaking during charging and discharging processes, and have high theoretical capacities and energy densities due to multi-electron contributions.^{45,46} Moreover, most of the conversion cathode materials focus on chalcogen monomers (S, Se, Te) and transition metal sulfides. In addition, the low cost and easy-to-control preparation process have also made the conversion cathode materials highly sought after by researchers.⁴⁷ Pan et al.⁴⁸ synthesized a CuS submicron sphere as a cathode for MIBs by high-speed centrifugation at low temperature, which can provide a high discharge capacity of 396 mAh g^{-1} at 20 mA g^{-1} and an excellent rate performance of 250 mAh g^{-1} at $1,000\text{ mA g}^{-1}$. Unfortunately, the discharge specific capacity rapidly decayed from 124 mAh g^{-1} to 35 mAh g^{-1} in 100 cycles at 100 mA g^{-1} , which is attributed to the structural collapse of the electrode material caused by the huge volume expansion brought about by the continuous crystalline phase transition. In order to alleviate this problem, researchers have designed various experimental processes to synthesize conversion cathode materials with excellent structures, such as core-shell, hollow, nanoflower, and other delicate structures through extensive research.⁴⁹ In this paper, we review the reports on the application of various sulfur-converted cathode materials for MIBs in recent years from the perspective of microstructure design, analyze the basic principles and advantages of each structural modification. Moreover, we provide an outlook on the current challenges faced by the transition metal-sulfides electrode materials and their future development directions, which is of inspiring significance for the structural design of the converted cathode materials for MIBs in the future.

Structure design of metal chalcogenide conversion-based cathode materials

In recent years, designing electrode materials into a wide variety of nanostructures has become a mainstream way for scientists to improve device performance.⁵⁰ Metal-ion batteries storage energy mainly through the repeated de-insertion of ions between the cathode and anode. Therefore, the insertion and de-insertion kinetics of metal ions in the electrode material have become an important indicator for evaluating the electrode material. At present, researchers have been able to shorten the diffusion path of Mg^{2+} in the material by modulating the morphology of sulfur-generic conversion analogues in various ways to achieve the effect of improving the mass transfer rate. Common nanostructure morphology includes nanoparticles, nanowires, self-assembled nanosheets, hollow and core-shell structures, etc. Among them, nanoparticles and self-assembled nanosheets have nanoscale particle sizes or ultrathin walls, which can not only shorten the ion diffusion paths drastically, accelerate the ion diffusion rate, and improve the insertion and de-insertion kinetics, but also can greatly increase the specific surface area of the material, accelerate the penetration of the electrolyte, shorten the activation cycle of the battery, and expose larger energy storage active sites to increase the actual discharge specific capacity of the material.⁵¹ Meanwhile, the self-assembled nanosheet structure possesses more buffer space between the thin walls, which can greatly alleviate the volume expansion of the conversion cathode material during the cycling process and prevent the collapse of the structure. Nazar et al.⁵² prepared several sulfide cathode materials such as layered TiS_2 and CuS at micron and nanometer scales, respectively, by varying the synthesis process and explored their effect on the electrochemical performance. It was shown that the electrochemical properties were positively modulated when the material size was reduced from micron to nanoscale. Specifically, the nanoscale WS-TiS_2 exhibited a 294 mAh g^{-1} higher discharge capacity and high stable capacity of 269 mAh g^{-1} after cycling. Meanwhile, WS-TiS_2 showed excellent stability in long-term cycling at 48 mA g^{-1} , maintaining 120 mAh g^{-1} at the 200th cycle. In comparison, the micron-scale TiS_2 only reached an initial discharge capacity of 270 mAh g^{-1} at 12 mA g^{-1} , which was substantially decayed to 160 mAh g^{-1} after further cycling. All these data fully illustrate the positive modulation of the electrochemical properties of the materials by nanosizing. Unfortunately, the nanoparticle morphology is prone to agglomeration during the preparation process due to excessive reactivity and low dispersibility of its system, which greatly reduces the specific surface area of the material.⁵³ In order to resolve this problem, researchers composite these excellent structures with diverse conductive carbon-basic materials such as reduced graphene oxide (rGO), carbon nanotubes (CNTs), etc., aiming to improve the electrical conductivity and accelerates the ionic conduction of the materials while promoting the dispersion of the nanostructures. Currently, composite C materials are prepared by *in situ* growth, precursor derivation, and carbon coating. Similarly, hollow, core-shell structures also have a special buffer space due to the large internal cavity with a

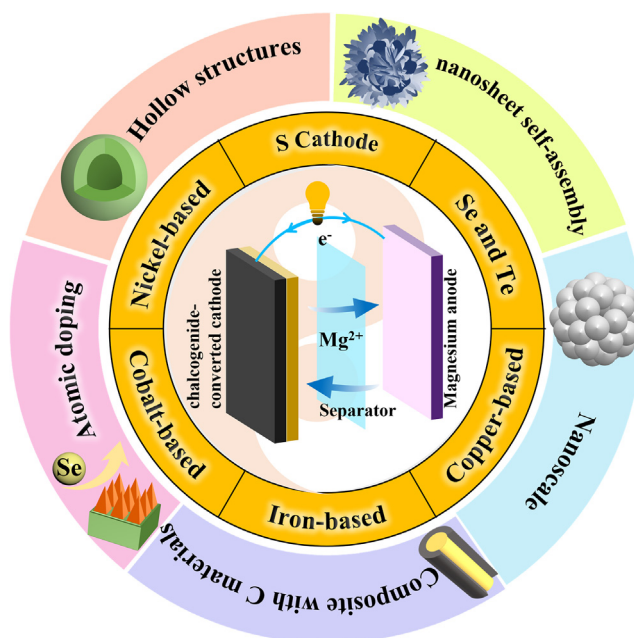


Figure 1. Schematic representation of sulphur-converted cathode materials in MIBs (design and construction of different micro-structures) overview

rigid outer shell, and are promising for applications in enhancing magnesium storage properties. In the following, each sulfur-genus conversion class cathode material is reported in detail in terms of structural design, and the advantages of each structure are analyzed in detail (Figure 1). Table 1 summarizes the key parameters of some reported chalcogenide conversion cathode materials for MIBs.

Cathode materials for MIBs

S cathode

S has received a lot of attention from the battery community due to its high natural reserves and high theoretical conversion capacity. Since 2009, the numerous advantages of S cathodes have sparked the research interest of researchers.⁶⁷ Initially, due to the more mature technology of LIBs, researchers first tried to apply S in the cathode material of LIBs. With the rising research and the development of various metal-ion batteries, a large number of research reports on the use of S cathode in other metal-ion batteries have appeared one after another, such as Na-S batteries, Mg-S batteries, and so on. The use of S as the cathode material for MIBs usually undergo a conversion reaction of two electrons with the theoretical capacity as high as 1684 Wh kg^{-1} .^{68,69} Unfortunately, the actual energy density of the S cathode falling far short of the theoretical value due to the extremely slow conversion kinetics caused by the low intrinsic conductivity of S and the discharge product MgS.^{70,71} In addition, the polysulfides produced by the S cathode during cycling pass through the diaphragm to the anode and form a passivation layer on the surface of the Mg anode. Laskowski et al.⁷² demonstrated that magnesium polysulfide is reduced to a MgS passivation layer at the anode thereby inhibiting the reduction of the Mg anode during charging by using an Ag_2S quasi-reference electrode in electrochemical tests to probe the interaction between the Mg anode and polysulfide. In response to these problems, researchers have proposed the following general solutions: (1) composite the S cathode with various conductive carbon substrates to increase the conductivity of the S cathode and improve its conversion kinetics; (2) partial doping of atoms such as Se, Te, and other homologous elements due to the longer covalent bonding lengths thereby broadening the charge transfer path, accelerating the ionic transport kinetics, and increasing the utilization rate of the S cathode.⁷³

Construction of S cathode and carbon substrate composites. In 2016, Fichtner et al.⁷⁴ employed a strategy of reducing polysulfides with formic acid to prepare high sulfur-loaded S-rGO composites with a sulfur loading of 49 wt %, followed by heat treatment of the product in argon gas to re-melt S into the interlayers and various pores of the rGO (Figure 2A). A high initial discharge capacity of 1024 mAh g^{-1} with an excellent reversible capacity of up to 448 mAh g^{-1} was obtained with Mg-C as the counter electrode. In addition, the device is stable at the 6th cycle of 20 mA g^{-1} , and the discharge specific capacity only decayed from 280 mAh g^{-1} to 219 mAh g^{-1} after 50 cycles, with a capacity retention rate of 78.2% (Figure 2B). The rGO matrix enhances the electrical conductivity of the composites and the abundant porosity provides a buffer space for the volume expansion of S. In addition, the adsorption and confinement of polysulfides by rGO also greatly improves the cycling ability of S. Even so, such discharge capacity and cycling performance are still not enough to meet the requirements of high-performance MIBs, so researchers have developed more excellent and novel structures based on this. Yu et al.⁷⁵ used S-filled preactivated carbon nanofibers (CNTs) as the cathode material and CNT-coated glass fiber membrane as a spacer for MIBs and obtained excellent electrochemical

Table 1. Summary of some key parameters of some reported chalcogenide conversion cathode materials for MIBs

Cathode material	Electrolyte	Current density (mA g ⁻¹)	Reversible Capacity (mAh g ⁻¹)	Cycling Performance	Potential (V)	Reference
S@MC	0.4 mol L ⁻¹ (PhMgCl) ₂ /AlCl ₃ + 1.0 mol L ⁻¹ LiCl/THF	10.026	224.7	0.16/200/368/37.5	0.5–1.7	Wang et al. ⁵⁴
Te@CSs	All-Phenyl Complex (APC)	100	350	0.1/500/229.7/77.1%	0.3–2.0	Chen et al. ⁵⁵
Ag ₂ S	Mg-HMDS-AlCl ₃	50	120	0.2/400/60/80%	0.1–2.5	Zhang et al. ⁵⁶
Ti ₃ C ₂ /CoSe ₂	0.4 M Mg ₂ Cl ₃ ⁺ ·AlPh ₂ Cl ₂ ⁻ /THF	50	96	0.05/500/96/80%	0.01–2.0	Liu et al. ⁵⁷
CuS-CTAB-2	0.3 M Mg[B(hfip) ₄] ₂ /DME	100	455	0.56/1000/111/65.2%	0.01–2.4	Shen et al. ⁵⁸
S-Cu _{2-x} Se	Mg-HMDS-AlCl ₃	100	200	0.2/300/109/65%	0.3–2.2	Chen et al. ⁵⁹
Cu _{2-x} Se-I	OMBB electrolyte	200	200	1/3500/114.9/85%	0.01–2.3	Zhao et al. ⁶⁰
Cu _{7.4} S ₄	MgHMDS-AlCl ₃	100	314	1/1600/59.1/82.5%	0.1–2.1	Yang et al. ⁶¹
NiS@C NPs/CC	APC-LiCl	100	437	0.2/250/214/61%	0.1–1.95	Zhu et al. ⁶²
Fe _{0.5} Co _{0.5} S ₂	MACC electrolyte	20	154	0.02/100/154/77%	0.5–2.5	Mao et al. ⁶³
CuCo ₂ S ₄	MgHMDS-AlCl ₃	50	154	0.5/100/392/88.4	0.1–2.1	Wang et al. ⁶⁴
Ex-Se-CuS NTs	MgHMDS-AlCl ₃	100	350	2/1600/64/61	0.1–2.1	Du et al. ⁶⁵
FeS ₂	0.3 M Mg[B(hfip) ₄] ₂ /DME	50	679	0.4/1000/90/60	0.01–2.5	Shen et al. ⁶⁶

Cycling Performance include: (1) Current density (A g⁻¹); (2) Cycle number (n); (3) Reversible capacity (mAh g⁻¹); (4) Capacity Retention (%).

performance, as shown in Figure 2D. Compared with the spacer without CNT coating, the Mg//CNF-GF//S with CNT coating showed more satisfactory discharge capacity and stability. Although both of them have similar discharge capacity in the first turn, from the second turn onwards, the discharge time per cycle of Mg//CNF-GF//S is significantly larger than that of Mg//GF//S and remains stable, while Mg//GF//S tends to decay rapidly along with the short discharge time (Figure 2E). In addition to this, Mg//CNF-GF//S also showed unprecedented rate performance, which exhibited similarly close to the ultra-high discharge specific capacity of 1000 mAh g⁻¹ at different current densities C/50, C/20, and C/10, and showed no significant capacity degradation over 20 charge/discharge cycles, which demonstrated a great potential for application. In this study, the conductive CNF coating on the separator was used both as an absorber layer to adsorb the diffused magnesium polysulfides and as a collector to electrochemically reuse the diffused magnesium polysulfides. This can be explained by the energy disperse spectroscopy (EDS) images of the CNT-coated layer after 20 cycles, and it can be found that the CNT layer after cycling still has a small portion of elemental S. This phenomenon indicates that the S in the cathode diffuses to the anode through the separator during the cycling process, which is additionally evidenced by a small amount of elemental S found on the surface of the Mg anode (Figure 2F). In addition, the porous nature of the CNT coating helped to absorb some of the polysulfides to enhance the cycling capacity of the Mg-S cell. Another benefit of the carbon nanofiber coating is that the voids of the carbon nanofibers can release stress and accommodate the volume change of the sulfur cathode during charging and discharging. In addition, Wang et al. ⁵⁴ obtained the composite S@MC in 2018 by melting sublimated sulfur into the pores of commercial microporous carbon (MC) by a simple ball-milling followed by melt-diffusion method (Figure 2G). The S@NC showed a sulfur content of up to 64.7%, which probably due to the high microporous distribution of MC. It was well known that high sulfur content is almost mandatory in achieving high bulk energy density in sulfur/carbon cathodes, but high sulfur loading simultaneously causes severe polarization, accelerates the shedding of S on the carbon substrate, and results in low active material utilization. Remarkably, S@NC achieves high sulfur loading while the microporous and highly conductive MC substrate greatly improves the electrochemical kinetics and locks the polysulfides well during cycling to prevent the infamous “shuttle effect”. Based on these advantages, S@MC exhibited a high initial discharge capacity of 979.0 mAh g⁻¹ and maintained a high capacity of 368.8 mAh g⁻¹ after 200 cycles at 0.1 C, showing improved sulfur utilization and cycling stability. When the current density is increased to 0.2 C, the S@MC composite still provides a capacity of about 200 mAh g⁻¹. Under the same conditions, the S without MC substrate maintained only a discharge capacity of 210.4 mAh g⁻¹ after 50 cycles. These data can be used to visualize the significant improvement of the electrochemical performance of the MC substrate (Figures 2H and 2I).

Atomic doping in S cathode. As we already know, S as a classical conversion cathode has excellent conversion capacity, but the development of S cathode is facing great difficulties due to its low conductivity and headache shuttle effect. Since elements such as Se and Te are in the same family with S and have similar properties with S, and have higher conductivity than S, therefore, combining Se or Te with S can theoretically improve the electrochemical performance of S, which provides a new exploration direction for researchers. Wang et al. ⁷⁶ fused elemental Se on the basis of the previous S@MC by firstly mixing S and Se powders homogeneously by ball milling and then melting them in a sealed vacuum glass tube to prevent accidental O doping and thus obtaining S-Se composites. Subsequently, the composite was ball-milled and calcined with ordered mesoporous carbon CMK₃ at a mass ratio of 4:1 to obtain the composite S_{0.96}Se_{0.04}@CMK₃. The electronic conductivity of the cathode material increased by 18 orders of magnitude after Se doping from 5 × 10⁻²⁸ to 6.5 × 10⁻¹⁰ S m⁻¹. This is very important for the improvement of electrochemical reaction kinetics of S cathode. It was found that the capacity of S_{0.96}Se_{0.04}@CMK₃ is slightly lower compared to S@CMK₃, which

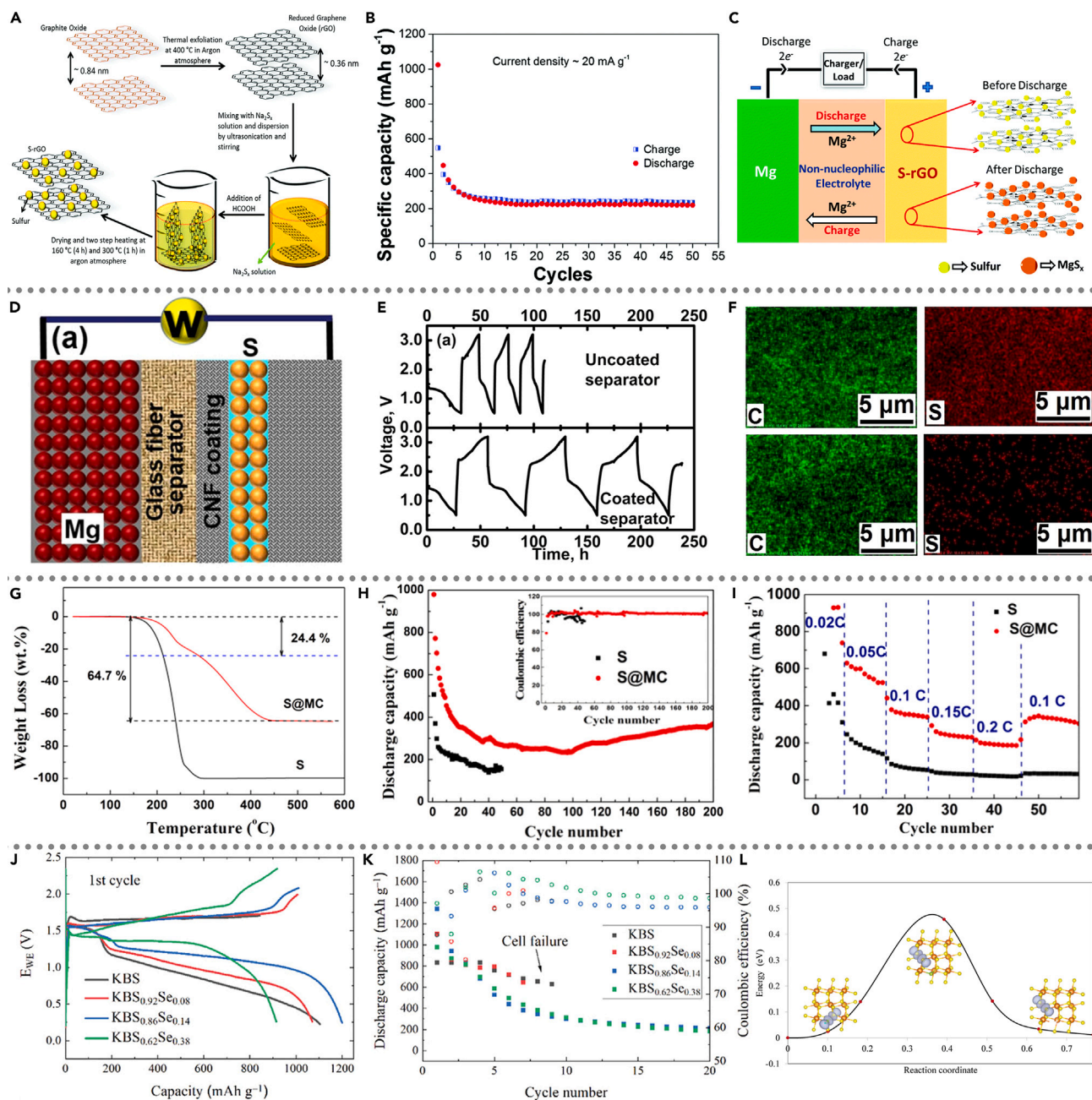


Figure 2. The application of S cathode material for MIBs

(A) Preparation process of S-rGO; (B) Short cycle performance of S-rGO; (C) Electrochemical mechanism of S-rGO nanocomposite electrode. Copyright 2016, Royal Society of Chemistry, Reproduced with permission.⁷⁴

(D) Schematic diagram of Mg-S cell with activated CNF-coated septum; (E) Voltage-time curves of Mg//CNF-GF//S and Mg//GF//S cells at C/50 rate; (F) EDS elemental (carbon and sulfur) plots of S/CNF electrode and CNF coating on the diaphragm after 20 cycles. Copyright 2016, American Chemical Society, Reproduced with permission.⁷⁵

(G) TGA curves of S@MC and S (H) Comparison of cycling performance; (I) Comparison of rate performance. Copyright 2018, Royal Society of Chemistry, Reproduced with permission.⁵⁴

(J) EWE vs. capacity in the first cycle; (K) KBS and cycling performance of KBS_{1-x}Se_x cathodes in a two-electrode button cell. (L) Magnetization densities in the initial, intermediate and final states of the minimum energy path for the diffusion of e⁻ polaritons in Se-doped MgSe₂. Mg, S, and Se atoms are shown in brown, yellow, and green. Copyright 2023, Wiley-VCH, Reproduced with permission.⁷³

is due to the lower theoretical capacity of Se compared to S. In spite of this, $S_{0.96}Se_{0.04}@CMK_3$ is significantly better than $S@CMK_3$ in terms of stability. In a short cycle of 0.1 C, the two materials show a similar decreasing trend in the first 40 cycles, with a slightly faster decreasing trend for $S@CMK_3$. From the 40th cycle, the discharge specific capacity of $S@CMK_3$ began to decay rapidly, decaying to 223.4 mAh g^{-1} after 110 cycles. In contrast, the $S_{0.96}Se_{0.04}@CMK_3$ exhibited extraordinary cycling stability, maintaining a high discharge specific capacity of 492.9 mAh g^{-1} after 110 cycles, with a capacity retention rate of an astonishing 96.4% from lap 45 onwards. When the current density is increased to 0.5 C, the $S_{0.96}Se_{0.04}@CMK_3$ can still stabilize at 429.8 mAh g^{-1} after 100 cycles, while the $S@CMK_3$ retains only 72.7 mAh g^{-1} . Although the doping amount of Se is small, the electronic conductivity of the S cathode is significantly improved, and its electrochemical kinetics is greatly improved. Mesoporous carbon also provides a conductive substrate for the S-Se cathode and mitigates the volume expansion during cycling. Combining all of the aforementioned structural advantages, $S_{0.96}Se_{0.04}@CMK_3$ material exhibits unprecedented performance.

Besides, Li et al.⁷³ also prepared a series of KBS, $KBS_{0.92}Se_{0.08}$, $KBS_{0.86}Se_{0.14}$, $KBS_{0.62}Se_{0.38}$ doping models with different S/Se ratios based on Ketjenblack (KB) by the classical ball milling and melting method, and discussed in detail the effect of Se as a modified additive on the S body. In the electrochemical performance test, $KBS_{0.86}Se_{0.14}$ was determined to be the optimal combination due to the highest discharge specific capacity and better cycling stability. In a galvanostatic charge/discharge (GCD) comparison at 0.1 C, $KBS_{0.86}Se_{0.14}$ shows a more pronounced discharge plateau than KBS and exhibits a high discharge capacity of 1200 mAh g^{-1} (Figure 2J). The $KBS_{0.86}Se_{0.14}$ could still maintain 200 cycles without short circuit after 200 cycles at 0.1 C. In contrast, the KBS cathode experienced early cell failure at the 10th cycle, which was mainly related to the anodic process, in which the polysulfides occurred shuttle effect on the surface of the Mg anode inducing inhomogeneous deposition of the Mg metal resulting in soft short-circuit occurrence (Figure 2K). This result can be explained by using *ex-situ* X-ray photoelectron spectroscopy (XPS) at both electrodes. During the first discharge of $KBS_{0.86}Se_{0.14}$ electrode, all the signal peaks typical of Se-S interactions with a peak of 163.8 eV singlet S, and a peak of 162.2 eV disappeared and transformed into new double peaks of 161.9 and 160.9 eV, which correspond to the S-S interaction of Mg polysulfide (MgS_n), S interactions and Mg-S interactions. The vanishing signals of S0 and the formation of MgS as the main product indicate the high utilization of S and hence the high capacity obtained. In contrast, there is still a large number of S0 species remain for the KBS cathode after the first cycle of complete discharge. Furthermore, the conversion is mainly limited to the polysulfide intermediate (strong S-S signal) rather than the final product (MgS), suggesting that S is only partially reduced. Density functional theory (DFT) calculations also demonstrated that the diffusion of the e' polariton exhibits a low migration barrier of 0.45 eV (i.e., 0.08 eV lower than that of the pure MgS_2), which suggests that the (S-Se)₂-dimer impurity may enhance the charge transport in MgS_2 . The low migration potential barrier indicates a high diffusion energy barrier for charge in it, which improves the performance of the cell (Figure 2L).

Se and Te cathodes

Researchers have made great efforts on Mg-S batteries, while studying the S cathode, Se, Te of the same family has also been directly used as the cathode active material of MIBs by researchers due to its superior conductivity and longer covalent bonding. Similar to the S cathode, the structure of Se, Te cathode is still mainly dominated by the composite of carbon materials. Fichtner and co-workers⁷⁷ used the melt-diffusion method to composite Se and solid solution SeS_2 with ordered mesoporous carbon CMK-3 to obtain $SeCMK-3$ and SeS_2CMK-3 composites and to investigate their electrochemical properties, respectively. As shown in Figure 3A, the $SeCMK-3$ cathode can provide a high specific capacity of 450 mAh g^{-1} at 0.2 C. In terms of rate performance, the discharge specific capacity of $SeCMK-3$ does not undergo a substantial decrease with increasing current density. Even at a high current density of 3C, the $SeCMK-3$ cathode can still provide 320 mAh g^{-1} . The excellent rate performance is attributed to the high electrical conductivity of the Se element, which results in accelerated kinetics of electrochemical reactions and higher utilization of active substances. *ex situ* Raman spectroscopy also demonstrated that the $SeCMK-3$ cathode underwent a phase transition from an electrically insulating Se_8 molecule encapsulated in a carbon matrix to a chained Se_n molecule with high electrical conductivity in the initial cycle and maintained its chain structure in the subsequent reversible conversion during the discharge/charge cycle (Figure 3C). This phase transition dramatically accelerated the kinetics of the redox reaction. For SeS_2CMK-3 , an initial discharge specific capacity of about 600 mAh g^{-1} was obtained in the voltage window of 0.5–2.5 V, which is higher than the initial capacity of the $SeCMK-3$ cathode (Figure 3D), demonstrating a new strategy to combine S-group elements into a solid solution without limiting to atomic doping to further increase the electrical conductivity and theoretical capacity.

Besides, a Te composite MC sphere cathode material was prepared by Zhi et al.⁵⁵ The microporous carbon sphere (CSs) was synthesized by emulsion polymerization of a super-crosslinked polystyrene sphere precursor and followed by carbonization at high temperature. Subsequently, Te powder and CSs were wet ball milled with high temperature calcination to obtain $Te@CSs$ composites. According to the results of thermogravimetric tests (Figure 3E), the Te loading of the composites reached 68.2%, which was attributed to the excellent microporous structure in the CSs host, and the high loading could greatly improve the energy density of the materials. As shown in Figure 3F, $Te@CSs$ exhibits a high initial discharge capacity of 447.6 mAh g^{-1} at 0.1 A g^{-1} , which stabilizes at 387 mAh g^{-1} after the second cycle. It remained at 331.8 mAh g^{-1} after 100 cycles, and the capacity retention rate reached 85.5%. It is worth noting that $Te@CSs$ can maintain a capacity of 165.4 mAh g^{-1} at 5 A g^{-1} , with good rate performance (Figure 3G). Moreover, the $Te@CSs$ electrode can maintain a discharge capacity of 229.7 mAh g^{-1} after 500 cycles at 0.5 A g^{-1} , and the capacity retention rate is as high as 77.1%. In contrast, the pure Te electrode experienced a sharp decline in capacity after 200 cycles, with a retention rate of only 17.5% (Figure 3H). The excellent cycling performance is due to the high conductivity of Te and well-structured CSs substrate. In addition, the two-step transformation process of $Te-MgTe_2-MgTe$ was revealed using advanced *in situ* X-ray diffraction (XRD) techniques (Figure 3I). Furthermore, the element mapping image after 100 cycles can be seen that the material still presents a regular spherical shape, indicating that the structure does not collapse during the cycle, and the uniform distribution of Mg elements also represents the effective embedding of Mg (Figure 3J).

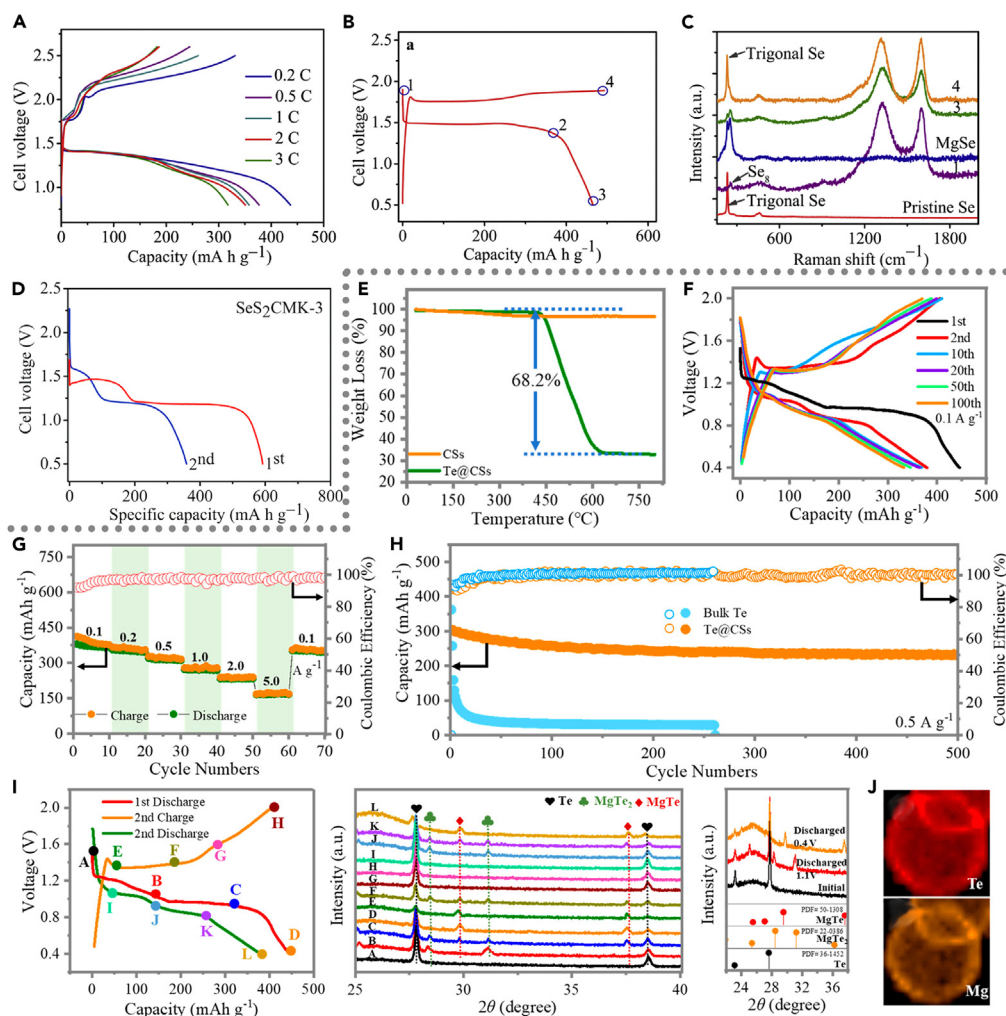


Figure 3. The application of Se and Te cathode material for MIBs

(A) Constant current discharge/charge curves of Mg-Se cells with different multiplicities in the voltage range of 0.8–2.8 V.

(B) First cycle discharge/charge curves of SeCMK-3 electrode at 20 mA g^{-1} .

(C) Raman spectra of Se cathode in different electrochemical states.

(D) Discharge curves of SeS_2 cathode in magnesium-based cells in the initial 2 cycles. Copyright 2016, Elsevier, Reproduced with permission.⁷⁷

(E) TGA curves of CSs and Te@CSs; electrochemical performance of Mg/Te cells: (F) GCD curves from 1 to 100 cycles at 0.1 A g^{-1} .

(G) Rate performance at different current densities (H) cycling performance and coulombic efficiency of Te@CSs and bulk Te; (I) GCD curves at 0.1 A g^{-1} with ex

situ XRD spectra at selected potentials and (J) elemental mapping of Te and Mg for Te@CSs electrode after 100 cycles. Copyright 2022, American Chemical Society, Reproduced with permission.⁵⁵

Overall, although pure sulfur genus monomers have ultra-high specific capacity, severe polysulfide shuttling effects tend to cause a rapid decrease in their energy storage capacity. In order to better confine the abnormally shuttled polysulfides/polyselenides and improve the magnesium storage capacity of sulfur genus elemental monomers, we can enhance the suppression of the volume expansion of the active materials by designing fine carbon encapsulation structures to improve the adsorption capacity of the polysulfides/polyselenides formed in the cycle. Besides, we cannot limit our vision to the modification of electrode materials, the functional design of separator and collector is also a good research direction. Synthesis of carbon-hybridized separator or introduction of adsorbent materials into the separator can also greatly enhance the adsorption capacity of polysulfides/polyselenides and improve the magnesium storage capacity of sulfur monomers.

Copper (Cu)-based chalcogenide cathodes

Cu-based chalcogenides (Cu_xT_y , T = S, Se) have attracted much attention due to their high theoretical capacity, stable charge-discharge platform and low cost. Since the development of MIBs, various Cu-based chalcogenides with excellent morphology have been synthesized and

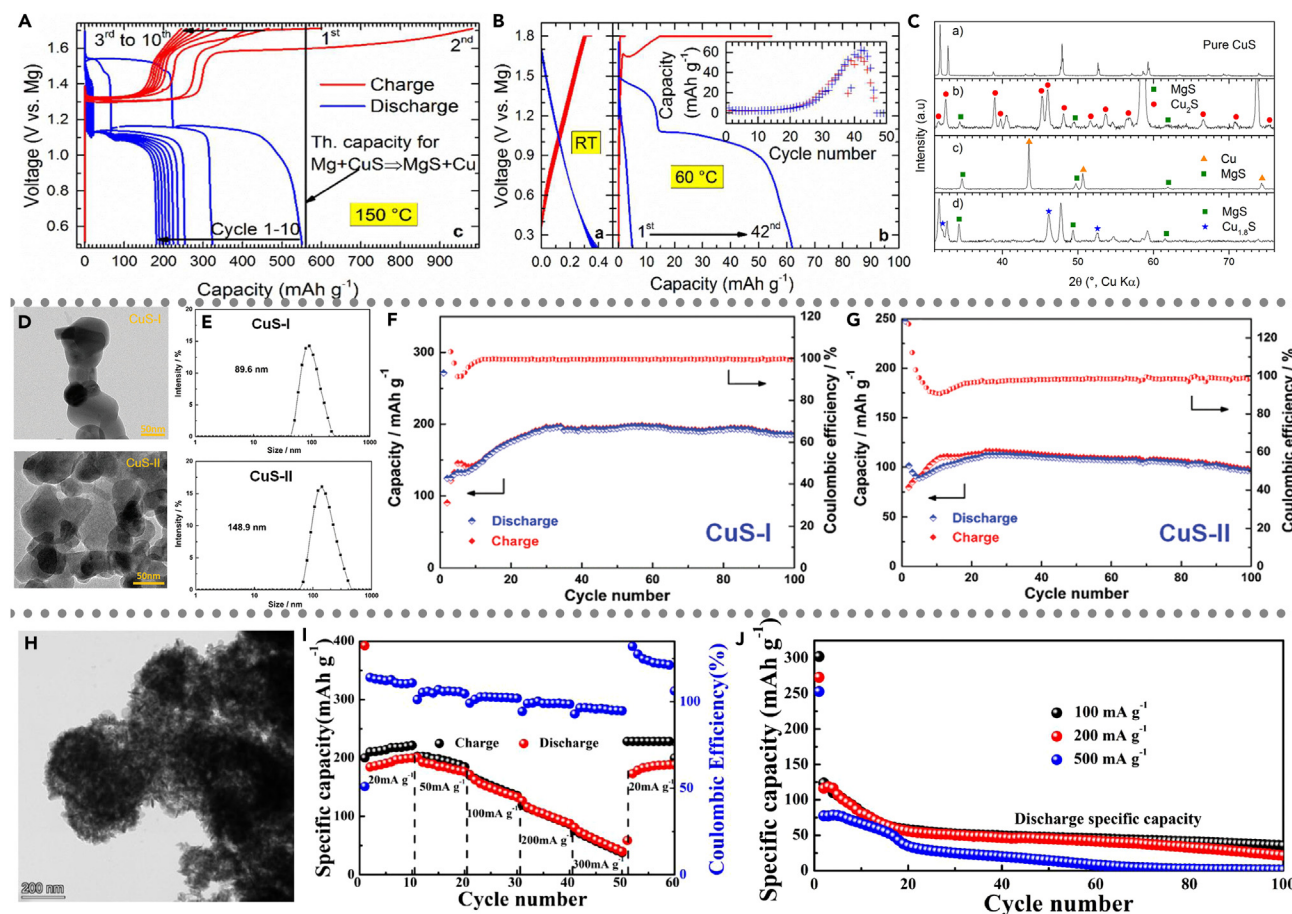


Figure 4. The nanoscale design of copper (Cu)-based chalcogenide cathodes for MIBs

(A) GCD curves of CuS cycled at each: 150°C, initial discharge close to the theoretical capacity (550 mAh g^{-1}); (B) room temperature vs. 60°C, the inset shows the trend of reversible capacity.

(C) XRD spectra of CuS cathode in different electrochemical states. Copyright 2016, Royal Society of Chemistry, Reproduced with permission.⁷⁹

(D and E) comparison of the Transmission Electron Microscopy (TEM) images (D) and DLS (E) of CuS-I, CuS-II.

(F) cycling performance graphs of CuS-I; (G) cycling performance graphs of CuS-II. Copyright 2018, Royal Society of Chemistry, Reproduced with permission.⁸⁰

(H) TEM images of CuS submicron spheres; (I) multiplicity performance graphs of CuS submicron spheres and (J) cycling ability at different current densities. Copyright 2023, Elsevier, Reproduced with permission.⁸¹

applied to MIBs cathodes, becoming the most popular conversion cathodes.⁷⁸ At present, the common Cu_xT_y compounds are CuS, Cu_2S , CuSe, Cu_2Se , CuSe_2 , and so on. Due to the high charge density of Mg^{2+} , the coulombic force between Mg^{2+} and S^{2-} is very large, which leads to the very slow magnesium storage reaction kinetics of CuS cathode, and the actual discharge capacity is far less than the theoretical capacity. Earlier, Duffort and co-workers⁷⁹ applied CuS cathodes in MIBs and explored their energy storage mechanism (Figures 4A–4C). They synthesized CuS nanoparticles with particle sizes of 5–10 μm by multi-step heat treatment of Cu powder with S powder. *ex situ* XRD revealed the electrochemical processes of two stable discharge platforms, which produced Cu_2S and MgS, and Cu and MgS, respectively (Figure 4C). Their capacities obtained at room temperature were negligibly low, and only about 10% of the theoretical capacity of the discharge capacity ($\sim 60 \text{ mAh g}^{-1}$) was obtained even when the temperature was raised to 60°C (Figure 4B). However, when the temperature was raised to 150°C, an initial discharge capacity close to the theoretical capacity was obtained, indicating that the high temperature environment accelerated the electrochemical reaction rate (Figure 4A). It can be seen that there is still a great potential to improve the performance of CuS in MIBs, and researchers need to put a lot of efforts for the application of CuS cathodes. By comparison, elemental Se has better electrical conductivity and smaller diffusion energy barriers for Mg^{2+} in selenide materials, and the coulombic interactions between the anions and cations of MgSe intermediates produced by Mg embedded in selenides are also smaller relative to MgS, which implies that less energy is required for detachment of Mg^{2+} during the charging process, greatly enhancing the reversibility of the insertion and de-insertion of Mg^{2+} in the materials. Thus, copper selenides show wider application prospects.

Unfortunately, copper-based sulfides still have problems such as low capacity, severe volume expansion due to constant reversible conversion reactions, and poor cyclic stability. Structural design is considered to be an effective way to solve these problems, and the general

solutions proposed by researchers are as follows: (1) employing various preparation strategies, such as hydrothermal/solvent-thermal, micro-blogging-assisted synthesis, precipitation, and template methods to synthesize materials with excellent morphology (hollow structures, nano-flowers, etc.) to improve the specific surface area and mechanical properties of the materials and thus improve their electrochemical properties; (2) the use of partially doping with homologous anions, which is the most common way to improve the electrochemical properties of copper-based sulfides. Part of the same group anion doping such as Se, Te, and other homologous elements due to longer covalent bond lengths thus broadening the charge transfer path, indirectly reduces the Mg^{2+} embedded in the host lattice when the coulombic force between the release, accelerating the reaction kinetics; (3) cation doping; (4) CuS nanostructures composite with a variety of conductive carbon substrate to improve the dispersion of its own electrical conductivity to enhance the conductivity. In addition, excellent carbon substrate structures can be designed to give the active materials enough buffer space to prevent rapid structural collapse caused by volume expansion during cycling. The previous aspects will be listed and discussed in detail in the following.

Nanoscale design. Xu et al.⁸⁰ investigated the effect of particle size on the MIBs performance by using two CuS (CuS-I, CuS-II) nanoparticles with different particle sizes. Both nanoparticles have particle sizes close to 100 nm, but a relatively large average particle size (148.9 nm) was observed for CuS-II. It was found that the smaller particle size provided a larger specific surface area ($10.8675 \text{ m}^2 \text{ g}^{-1}$ for CuS-I, $6.6503 \text{ m}^2 \text{ g}^{-1}$ for CuS-II), which contributed to the full exposure of the active sites to enhance the reactivity (Figures 4D and 4E). By comparison, the CuS-I with smaller particle size exhibits a stable capacity of around 200 mAh g^{-1} at 50 mA g^{-1} after some activation process. In contrast, CuS-II only showed a capacity of $\sim 120 \text{ mAh g}^{-1}$ and poor cycling performance, decaying to 90 mAh g^{-1} after 100 cycles, which is more prone to agglomeration during cycling leading to the hiding of active sites, resulting in the rapid decay of the capacity (Figures 4F and 4G).

Recently, Pan et al.⁸¹ prepared a CuS nanorods with a particle size of 250 nm by low-temperature synthesis method using copper nitrate and sodium thiosulfate in ethylene glycol with low-temperature stirring. The acicular morphology of the surface greatly improved the specific surface area of the material, which led to excellent rate properties (Figure 4H). The high specific capacity of 396 mAh g^{-1} at 20 mA g^{-1} and a remarkable rate capacity of 250 mAh g^{-1} at 1000 mA g^{-1} are attributed to the excellent morphology features (Figure 4I). Thus, the effect of nanosizing the converted material on the electrochemical properties cannot be underestimated, and small particle size has a significant effect on the physical properties of the material. Moreover, nanosizing the material also reduces the agglomeration phenomenon of the material during cycling, which is an effective material modification strategy.

Nanoflower and nanosheet self-assembly. Generally, changing the solvent (water) in the hydrothermal system to other organic solvents can change the morphology of the product to a certain extent. Therefore, many researchers have synthesized a large number of microstructures with the morphology of nanoflowers or self-assembled nanosheets and spheres using solvothermal reaction. Commonly used solvents in the reaction include ethanol, ethylene glycol, dimethyl formamide (DMF), oleylamine, etc., and common surfactants are polyvinyl pyrrolidone (PVP), cetyltrimethylammonium bromide (CTAB), sodium dodecyl sulfate (SDS), etc. The main mechanism for the formation of this morphology is that the micelles formed by the surfactant in water cover the surface of the nuclei, resulting in a change in the growth rate of the individual crystal surfaces, with the faster-growing orientations becoming outwardly protruding and forming many folds. The wrinkled surface and vertically oriented nanosheets provide the material with a huge specific surface area, which facilitates the rapid penetration of the electrolyte and shortens the activation time of the material. On the other hand, the large specific surface area also exposes a large number of active sites, which improves the reactivity of the material and increases the actual discharge capacity. In addition, the dense vertical nanosheets also provide rigid support for the structure, avoiding the structural collapse of the nanostructures under long-term high-current impact.

Cao's group⁸² used different solvents and reaction conditions to prepare conventional CuS nanoparticles and CuS with exquisite nanoflower ball morphology using solvothermal reaction, and further investigated the effect of morphology on the electrochemical properties of the materials. Firstly, CuS nanoparticles was synthesized without surfactant using $\text{Cu}(\text{NO}_3)_2 \cdot 6\text{H}_2\text{O}$ as a copper source and sulfur powder as a sulfur source, as well as ethylene glycol as a solvent. Exquisite single crystal CuS nanorods were synthesized using a mixture of acetone and water as mixed solvent and thiourea as sulfur source in the presence of dual surfactants (PVP and CTAB) (Figure 5A). The large number of vertical nanosheet arrays enabled the CuS nanoflower spheres to have a large specific surface area ($9.3 \text{ m}^2 \text{ g}^{-1}$, 4.69 m^2 for CuS nanoparticles) with a large number of microporous mesoporous structures. Based on these structural features, the CuS nanoflower spheres shown in Figure 5D exhibited a high specific capacity of 252 mAh g^{-1} at 0.1 A g^{-1} and a reversible specific capacity of 171.2 mAh g^{-1} at 0.5 A g^{-1} . In addition, the CuS nanoflower spheres still possessed a specific capacity of 91.7 mAh g^{-1} at a high current of 1 A g^{-1} and could be stable for 500 cycles with a capacity retention rate of 83.3%. In contrast, the CuS nanoparticles only exhibited a low discharge capacity of less than 100 mAh g^{-1} at 0.2 A g^{-1} (Figure 5F). The large pores between the nanosheets in the CuS nanoflower spheres provided buffer space for the cathode material during cycling, which greatly improved its cycling stability. In addition, Cao et al.⁸³ synthesized single-crystalline CuSe nanosheet self-assembled spheres with high (110) crystallographic orientation by advanced microwave-assisted synthesis method using $\text{Cu}(\text{CH}_3\text{COO})_2 \cdot \text{H}_2\text{O}$ as a copper source, SeO_2 as a selenium source, and oleylamine as a solvent (Figures 5G–5I). The prepared CuSe nanosheet spheres presented an initial discharge capacity of up to 600 mAh g^{-1} at a current density of 0.2 mA g^{-1} , which was maintained at 204 mAh g^{-1} after stabilization (Figure 5J). Moreover, a specific capacity of 48 mAh g^{-1} at 1 A g^{-1} was still achieved after 700 cycles, with a capacity decay of only 0.095% per cycle. Compared to polycrystalline nanoparticles, the CuSe nanosheet spheres show more excellent rate performance with higher capacity at each current density. In addition, TEM tests were carried out on single-crystal CuSe nanoflower spheres after cycling for ten cycles, and the flower-like morphology was not damaged under the fully discharged state, and the initial morphology was well

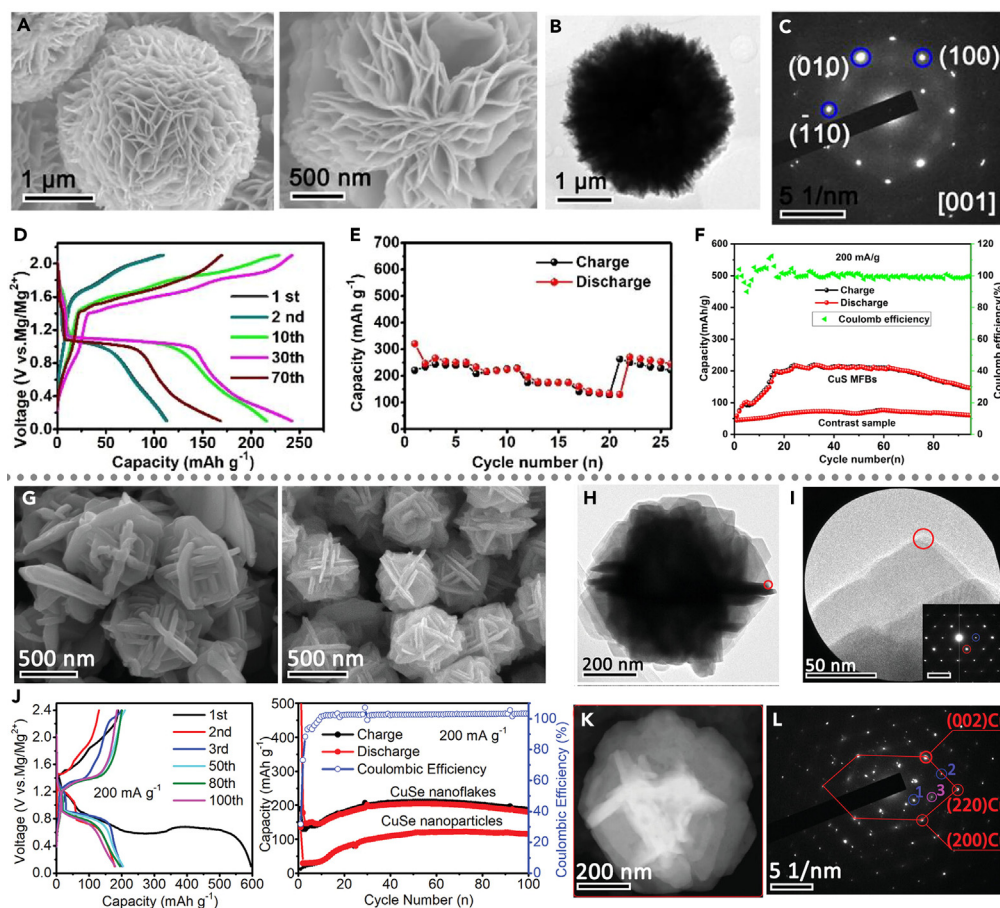


Figure 5. The nanoflower and nanosheet self-assembly copper (Cu)-based chalcogenide cathodes for MIBs

(A) SEM images, (B) TEM images and (C) selected electron diffraction image of CuS nanoflowering spheres.

(D) GCD curves, (E) rate performance and (F) the cycling performance of CuS material. Copyright 2021, Elsevier, Reproduced with permission.⁸²

(G and H) SEM images of CuSe nano-flowering spheres at different magnifications (G) and TEM images (H).

(I) selected electron diffraction images and (J) GCD curves with different number of cycling turns in comparison with the cycling performance of CuSe nanoparticles.

(K and L) TEM images after 10 times of deep charging and discharging with (L) selected electron diffraction images. Copyright 2021, Wiley-VCH, Reproduced with permission.⁸³

maintained (Figure 5K-5L). Selected electron diffraction also strongly confirms that the CuSe still presents a good single-crystal structure after cycling, which proves the role of single-crystal structure in the maintenance of the material morphology, and provides an effective suggestion for the structural design of electrode materials.

Hollow structures. In addition to the nanoflower morphology discussed in the previous section, the hollow structure is considered to be one of the effective strategies to improve the cycling performance of electrode materials due to the feature that the huge volume cavities provide a huge buffer space for volume expansion and can withstand the stresses generated during larger cycling. For Cu-based chalcogenides, researchers have obtained a series of hollow nanosheet self-assembled nano cubes with excellent morphology by using Cu₂O precursor as a hard template, and growing CuS, CuSe nanosheets and other structures on its outer surface through *in situ* selenide sulfurization and other strategies, and then removing the hard template by chemical treatment, which have obtained satisfactory electrochemical performances. This provides a simple yet ingenious morphology preparation strategy for the preparation of sulfur genus compounds.

Xu et al.⁸⁴ utilized sodium citrate as a soft template to produce Cu(OH)₂ cube precursors by precipitation of Cu²⁺ with a base in a dilute solution, and then added ascorbic acid as a mild reducing agent to gradually reduce the Cu(OH)₂ cube to a Cu₂O template during stirring. Cu⁺ has high reactivity and can react with S²⁻, Se²⁻, etc. to generate corresponding compounds easily at room temperature. Then, Cu₂O was dispersed in different concentrations of Na₂S solution to form a CuS capping layer on the outer side by stirring, and then the template in the center was removed by NH₃·H₂O to obtain the CuS hollow cubes (Figure 6A). By comparison, it was found that the higher the concentration of the sulfur source solution, the larger the particle size of the formed product (Figure 6D). The (Brunauer–Emmett–Teller) BET results showed

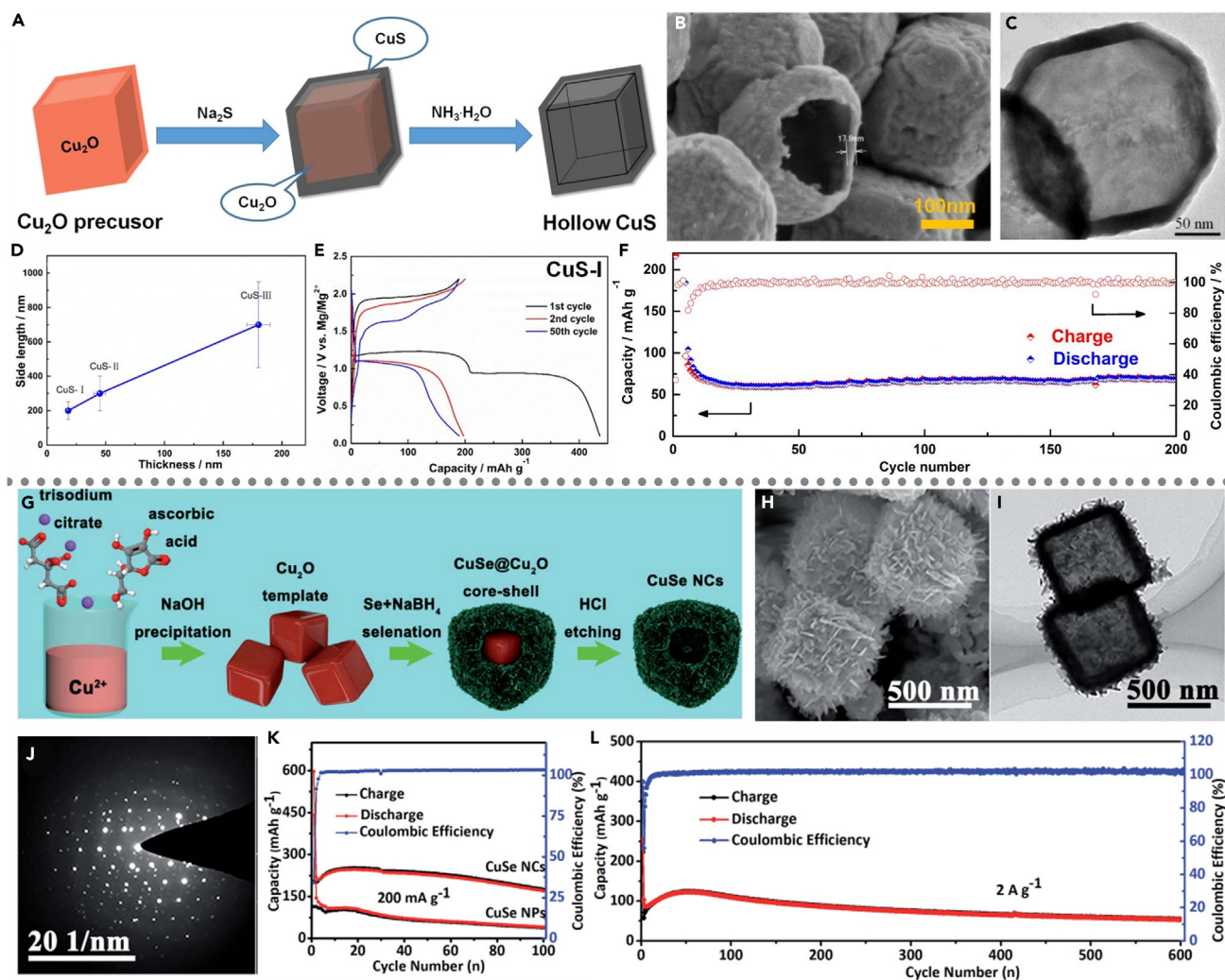


Figure 6. The hollow structures of copper (Cu)-based chalcogenide cathodes for MIBs

(A–C) Preparation schematic(A) and SEM image(B) and TEM image(C) of CuS hollow cubes.

(D) particle size comparison curves of different CuS; (E and F) GCD curve(E) (CuS-I) and long cycling performance (F). Copyright 2019, Royal Society of Chemistry, Reproduced with permission.⁸⁴

(G) Preparation schematic of CuSe nanosheet self-assembled hollow cubes; (H) SEM image; (I) TEM image and (J) selected electron diffraction; (K) comparison of cycling performance with CuSe nanoparticles; (L) long cycling performance. Copyright 2021, Royal Society of Chemistry, Reproduced with permission.⁸⁵

that the CuS-I with the small particle size possessed the large specific surface area of $198.474 \text{ m}^2 \text{ g}^{-1}$. Thus, CuS-I showed the excellent electrochemical performance with a reversible capacity of about 200 mAh g^{-1} at 0.1 A g^{-1} , which also shows the positive effect of large specific surface area and small particle size on the energy storage capacity (Figure 6E). It is noteworthy that all three CuS have good cycling stability with almost no capacity loss in 50 cycles. Among which, CuS-I can be stably cycled for 200 cycles with almost no capacity loss at 1 A g^{-1} , and this excellent cycling performance is attributed to its excellent hollow structure (Figure 6F).

Beyond that, Cao et al.⁸⁵ in 2021 used a similar approach to synthesize hollow CuSe by replacing the sulfur source with a selenium source. They reduced the Se powder to highly reactive Se^{2-} using NaBH_4 , and under stirring Se^{2-} quickly combined with the Cu_2O template to generate a CuSe nanosheet self-assembled shell layer in the outer layer. Finally, the self-assembled morphology of the hollow CuSe single-crystalline nanosheets was obtained after treatment by dilute hydrochloric acid (Figures 6G–6J). It obtained a stable high discharge capacity of 252 mAh g^{-1} at 0.2 A g^{-1} and still maintained 170 mAh g^{-1} after 100 cycles. In contrast, CuSe nanoparticles only obtained a discharge capacity of 177.7 mAh g^{-1} and rapidly decayed to 40 mAh g^{-1} in 100 cycles (Figure 6K). The excellent cycling stability of the CuSe nano cubes was attributed to the dual modulation of their huge cavities and nanosheet morphology, where the nanosheets improved the contact with the electrolyte and the large cavities mitigated the stress damage. In addition, the CuSe nano cubes activated to a maximum capacity of 122.7 mAh g^{-1} after 46 cycles at 2 A g^{-1} and remained at 52.6 mAh g^{-1} after 600 cycles, with only 0.115% decay per cycle (Figure 6L).

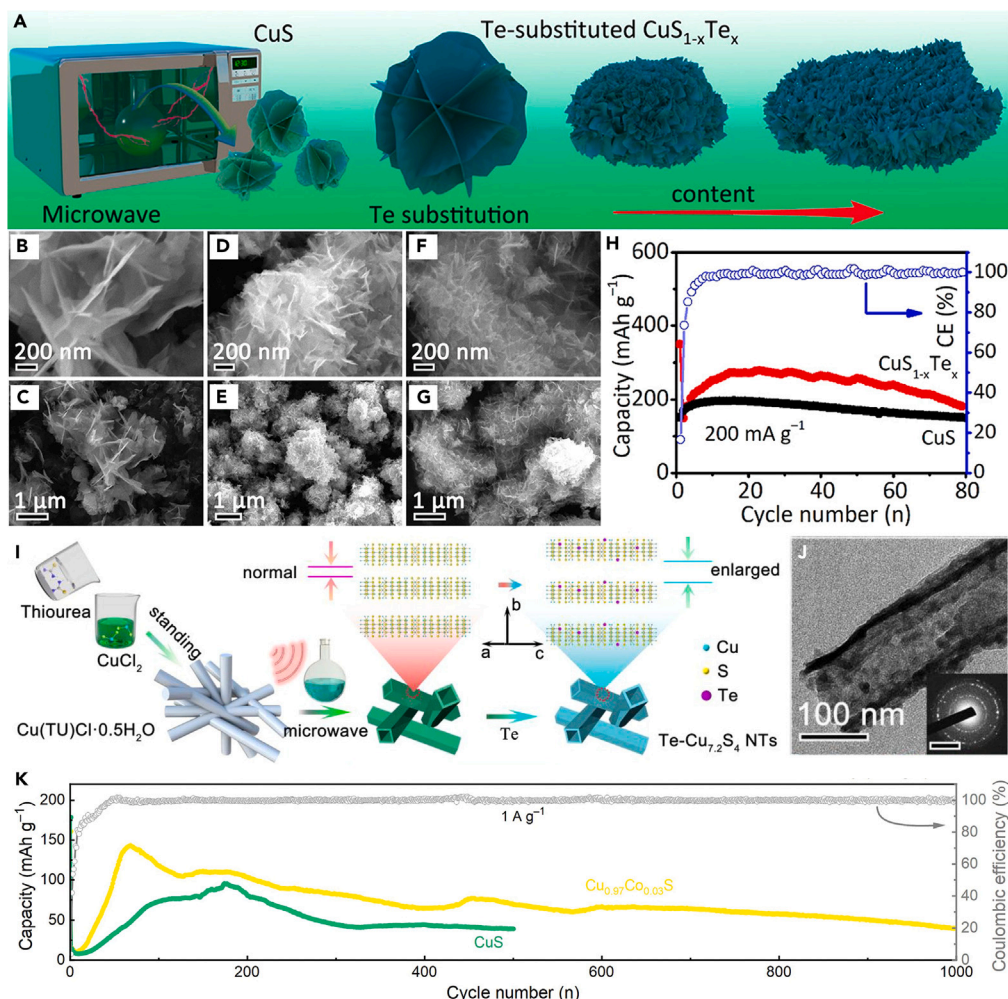


Figure 7. The Atomic doping of copper (Cu)-based chalcogenide cathodes for MIBs

(A) Schematic of CuS_{1-x}Te_x preparation. SEM images of (B and C) CuS_{0.96}Te_{0.04}, (D and E) CuS_{0.78}Te_{0.22}, (F and G) CuS_{0.77}Te_{0.23}.

(H) Cycling properties at 0.2 A g⁻¹. Copyright 2022, American Chemical Society, Reproduced with permission.⁸⁶

(I and J) Schematic of the synthesis route of pristine and Te-substituted Cu_{7.2}S₄ nanotubes (I) and TEM images (J). Copyright 2023, Elsevier, Reproduced with permission.⁸⁷

(K) Long cycling performance of Co cation co-doped CuS nanosheet cathode compared with pristine CuS. Copyright 2023, Elsevier, Reproduced with permission.⁸⁸

Atomic doping. After a long period of exploration, researchers have found that modulating the chemical properties of anions is an important process for improving the electrochemical properties of converted sulfur compound cathode materials. Anion substitution using some larger anions with higher polarization rates can greatly improve the electrical conductivity of the raw material, and widening the lattice spacing makes the ion diffusion barrier lower. Among the chalcogen elements, Se, Te, and other elements are often used as anion doping sources due to their large size and high conductivity, and the anion-substituted cathode materials have shown satisfactory magnesium storage properties.

Cao et al.⁸⁶ used thioacetamide (TAA) as a sulfur source, Na₂TeO₃ as a tellurium source, and CuCl₂ as a copper source in ethylene glycol to rapidly synthesize Te-substituted CuS nanoflowers by an advanced microwave-assisted synthesis method (Figure 7A). By characterization, the micro sheets on the surface of the material become smaller and densely arranged as the substitution of Te increases, which is conducive to the increase of the specific surface area of the material. HRTEM and XRD show that Te substitution leads to a small enlargement of the (102) crystal plane spacing and a significant reduction of the (110) crystal planes, which is a powerful crystal structure tuning strategy (Figures 7B–7G). The Te-substituted CuS_{1-x}Te_x nanoflowers exhibited a high stable capacity of about 270 mAh g⁻¹ at 0.2 A g⁻¹ and can be stably cycled for 80 cycles. Its capacity was higher than that of pure CuS nanoflakes in all 300 cycles at 0.5 A g⁻¹, only decaying from 336.9 mAh g⁻¹ to 114.8 mAh g⁻¹ with a capacity retention of 34% (Figure 7H).

In recent years, Cao et al.⁸⁷ did a similar research work based on the previous work. They chose a cation-rich Cu_{7.2}S₄ as the main cathode material, and the fast and efficient Cu⁺ migration rate makes Cu_{7.2}S₄ more promising. On this basis, Cao et al. likewise attempted to change

the crystal structure of the initial material through the anionic substitution of Te to obtain more prominent electrochemical properties. In the presence of microwaves, ethylenediamine was used as an etchant to evolve Cu(TU)Cl·0.5H₂O precursor nanorods into Te-substituted Cu_{7.2}S₄ hollow nanotubes (Figure 7I). It exhibited an ultra-high discharge capacity of about 350 mAh g⁻¹ after stabilization at 0.1 A g⁻¹ and could be stable for 60 cycles. Among them, 0.2Te-Cu_{7.2}S₄ with a molar ratio of 1:5 exhibited the highest discharge capacity and rate performance. Besides, 0.2Te-Cu_{7.2}S₄ still maintains a high capacity close to 50 mAh g⁻¹ after 2000 cycles at 2 A g⁻¹, indicating that the anionic substitution strategy of Te greatly enhances the long cycling capability of Cu_{7.2}S₄. In addition to anion substitution to adjust the lattice structure, Cao's group also explored the effect of cation co-doping on the magnesium storage properties of CuS nanoflowers during the same period.⁸⁸ Co-substituted Cu_{1-x}Co_xS nanosheets were synthesized by dissolving cobalt and copper salts in ethylene glycol as a bimetallic source and adding thiourea as a sulfur source under the powerful energy of microwave. Compared with undoped CuS, Cu_{1-x}Co_xS showed shorter activation cycle with higher specific capacity. Especially, Cu_{0.97}Co_{0.03}S obtained the highest capacity of 300 mAh g⁻¹ after 15 cycles of activation at 0.2 A g⁻¹, whereas undoped CuS showed 200 mAh g⁻¹ discharge capacity only after 45 cycles. The co-doping of Co greatly improves the Mg²⁺ magnesium storage kinetics of CuS and shortens the activation cycle. In the cycling test, Cu_{1-x}Co_xS exhibits a high stable capacity of nearly 150 mAh g⁻¹ at 1 A g⁻¹ and maintains a high capacity of 50 mAh g⁻¹ after 1000 cycles, showing excellent cycling performance (Figure 7K).

Iron (Fe)-based sulfides

Pyrite (FeS₂), with high natural reserves, simple synthesis, and a theoretical capacity of up to 896 mAh g⁻¹, is considered to be a very promising high energy density cathode material for MIBs. However, there are relatively few reports on FeS₂ in MIBs, and the magnesium storage mechanism of FeS₂ is scarce. Therefore, it is necessary to develop high-performance FeS₂ cathode materials and reveal the energy storage mechanisms. Unfortunately, the FeS₂ cathode material prepared by Mao et al.⁶³ in 2020 only obtained a stable discharge capacity close to 40 mAh g⁻¹, exhibiting low electrochemical activity. Currently, researchers are mainly focusing on the enhancement of the electrochemical performance of the materials through atomic doping, which is usually achieved by adjusting the ratio of precursor to dopant, and controllable and quantitative doping can be achieved during hydrothermal or thermal treatments. Xu et al.⁸⁹ hydrothermally synthesized Fe_{1-x}Co_xS₂ with different Co doping ratios in a mixed solvent of DMF and ethylene glycol by adjusting the ratio of iron and cobalt sources (Figure 8A). Various characterizations revealed that the Fe_{1-x}Co_xS₂ particle size gradually decreases with increasing Co doping, the lattice spacing gradually expands and the crystallinity gradually decreases. This structural evolution is conducive to increasing the electrochemically active area of the cathode material and enhancing the electrochemical performance (Figure 8B). Meanwhile, the report proposed a non-nucleophilic phenol-based magnesium complex (PMC) electrolyte with high sulfur genus compound matching, and the modified material obtained an ultra-high discharge capacity of 700 mAh g⁻¹ in PMC electrolyte system, which has exceeded the majority of MIBs cathode materials reported so far, and it is of great significance for research (Figure 8C). With the increase of Co doping, the capacity was gradually increased and the cycling ability was gradually improved. In which, Fe_{0.5}Co_{0.5}S₂ showed a high discharge capacity of 249 mAh g⁻¹ after more than 400 activated process at 1 A g⁻¹ and retained a high capacity of about 200 mAh g⁻¹ after nearly 600 subsequent cycles, with a capacity retention rate of 80.3% (Figure 8D). It can be seen that the effect of cation doping on the modification of electrode materials is immediate, which provides excellent modification ideas for the development of high-performance electrode materials. Most critically, the authors monitored the Cu_{1.8}S physical phase in the post-cycling electrodes through a series of *in situ* characterizations, which strongly suggests that the Cu species on the Cu collector gradually infiltrate into the electrode material, providing the material with a continuous favorable electronic pathway. This also provides a brand new idea for researchers to study the energy storage mechanism of sulfur genus compounds. In addition, the matching of electrolyte and electrode materials is a crucial issue for the development of high-performance MIBs, and both should be taken into account in the development of MIBs. Thus, the development of high-performance electrode materials needs to be thought about in the development of matching electrolyte system at the same time.⁹⁰

In addition to this, Wang et al.⁹¹ synthesized FeS₂ porous nanosheets by the solvothermal reaction of iron acetylacetonate with TAA in isopropanol, and then calcined at high temperature to obtain the final S-FeS₂ product (Figure 8E). According to multiple physical characterizations, the material undergoes a partial phase transition from mica to pyrite during the calcination process with increased grain size and enhanced crystallinity. This phase transition simultaneously gives the material both the high electrical conductivity of martensitic FeS₂ and the strong stability of pyrite FeS₂, mitigating the stronger shuttle effect of the pristine FeS₂ and greatly enhancing the material's magnesium storage properties (Figures 8F and 8G). The heat-treated S-FeS₂ obtained an ultra-high discharge capacity of 580 mAh g⁻¹ after 60 cycles at a current density of 25 mA g⁻¹ and remained stable for the next 20 cycles (Figure 8H). In contrast, the uncalcined FeS₂ experienced an overcharge short-circuit at 31 cycles and was less stable, while the commercial pyrite FeS₂ only obtained a capacity of less than 10 mAh g⁻¹, which further illustrates the reported great impact on the excellent structural design of FeS₂.

Cobalt-based sulfides

In addition to iron-based sulfides, cobalt-based materials also show strong application prospects in MIBs due to their abundant natural reserves and high electrical conductivity. In recent years, there are relatively few reports on cobalt-based materials, and a lot of research is needed to explain their deeper mechanisms. At present, the development of electrode materials for cobalt-based sulfides mainly focuses on nanosizing, surfactant-induced morphology formation, and compositing with carbon materials.

Cai et al.⁹² first applied spinel-structured Co₃S₄ in MIBs. They used the solvothermal reaction of Co (OAc)₂·4H₂O with TAA to synthesize nanoflower spheres (Co₃S₄-F) in a laminated nanosheet self-assembled structure, and the thickness of the nanosheets was small at only

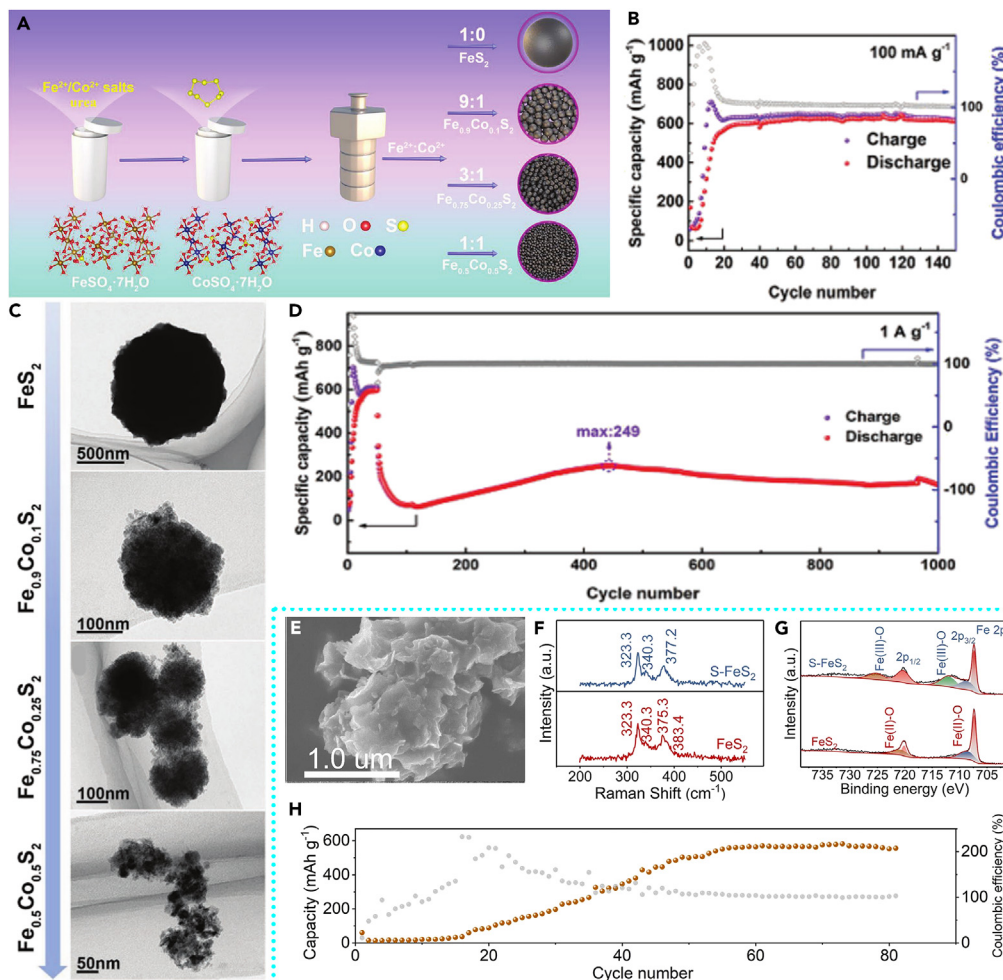


Figure 8. The application of iron (Fe)-based sulfides cathode for MIBs

(A) Schematic diagram of $\text{Fe}_{1-x}\text{Co}_x\text{S}_2$ preparation.

(B) TEM images corresponding to different doping amounts of $\text{Fe}_{1-x}\text{Co}_x\text{S}_2$.

(C and D) cycling performance of $\text{Fe}_{0.5}\text{Co}_{0.5}\text{S}_2$ at 0.1 A g^{-1} (C) and 1 A g^{-1} (D). Copyright 2022, Wiley-VCH, Reproduced with permission.⁸⁹

(E–G) SEM images of S- FeS_2 (E) and Raman spectra (F) and XPS spectra (G) of S- FeS_2 and FeS_2 ; (H) cycling performance of S- FeS_2 at 25 mA g^{-1} . Copyright 2024, Elsevier, Reproduced with permission.⁹¹

10 nm, which considerably shortened the diffusion of Mg^{2+} pathway (Figure 9A). The strategy of heat-treating the sulfurized Co_3O_4 precursor was also used to synthesize hierarchically mounted nanorods (Co_3S_4 -T) and explore the Mg storage properties separately (Figure 9B). As shown in Figure 9C, the Co_3S_4 -F electrode obtained an excellent initial discharge capacity of 779.8 mAh g^{-1} in the APC/LiCl electrolyte system at 100 mA g^{-1} , and still maintained a 399.5 mAh g^{-1} even after 100 charge/discharge cycles, with a high-capacity retention rate of 51.2%. Interestingly, the capacity of Co_3S_4 -T was only 16.9 mAh g^{-1} after 100 cycles. The experimental results show that the nanoscale plays an important role in the storage capacity of Mg^{2+} , which provides an important guideline for the preparation and development of conversion cathode materials.

In addition to changing the solvent and temperature of the solvothermal reaction and using precursors to adjust the crystal morphology, the inducing effect of surfactants in the crystal growth process is often twice as effective. Gao and co-workers⁹³ reported a method to induce the growth of $\text{Co}_{0.85}\text{Se}$ nanosheets by using CTAB as a surfactant. The $\text{Co}_{0.85}\text{Se}$ added with CTAB evolved from a bulk morphology to a nanosheet morphology compared with the comparison sample, and the particle size was reduced while the dispersibility was greatly increased, which led to a significant increase in the electrolyte wettability of the material, and made a positive contribution to the enhancement of the magnesium capacity for storage and rate performance. It is a positive contribution to the improvement of magnesium storage capacity and rate performance. As shown in Figures 9E and 9F, $\text{Co}_{0.85}\text{Se}$ -CTAB showed a high capacity of 93 mAh g^{-1} at 0.05 A g^{-1} , whereas the comparison sample, $\text{Co}_{0.85}\text{Se}$, only showed a capacity of 53 mAh g^{-1} . This result confirms our prediction based on the surfactant-modulated structure and reveals the universality of surfactants for the performance enhancement of electrode materials.

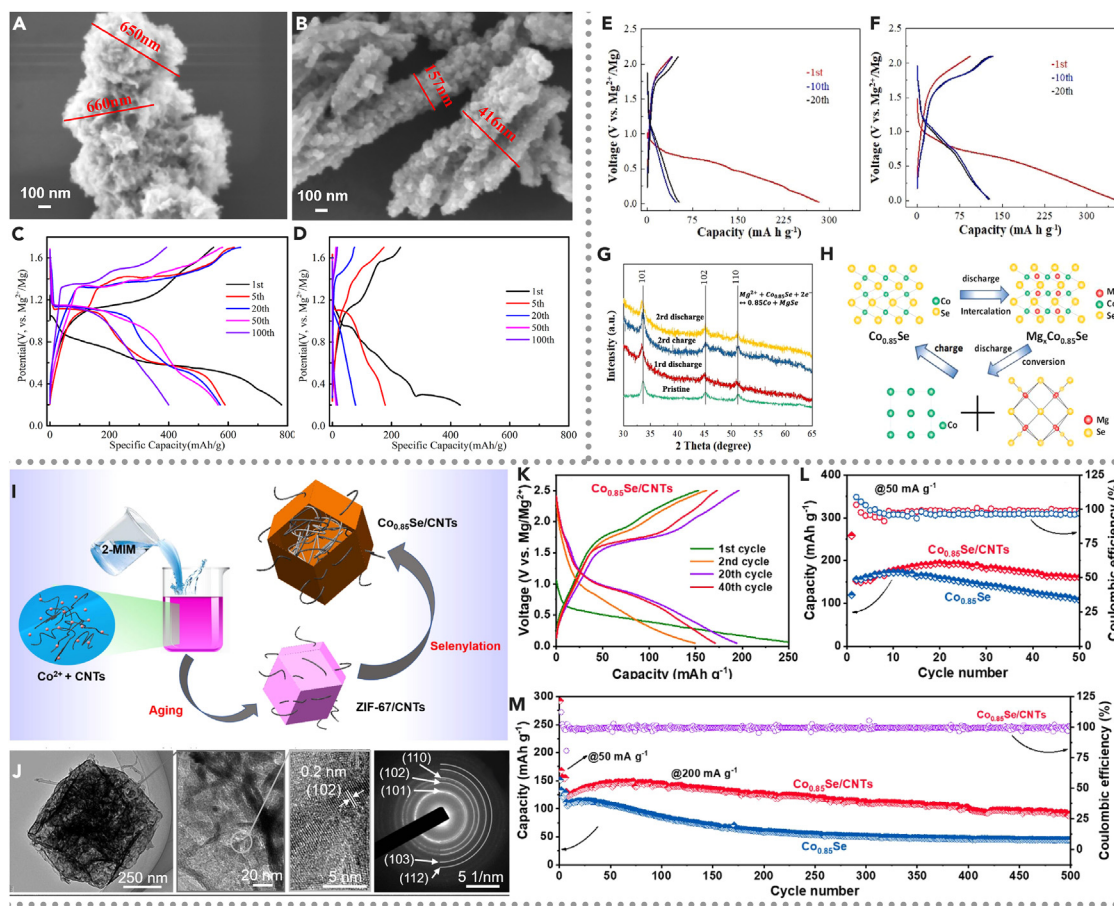


Figure 9. The application of cobalt-based sulfides cathode for MIBs

(A and B) SEM images of granular $\text{Co}_3\text{S}_4\text{-F}$ (A) and rod $\text{Co}_3\text{S}_4\text{-T}$ samples (B).

(C and D) GCD curves of granular $\text{Co}_3\text{S}_4\text{-F}$ (C) and rod-like $\text{Co}_3\text{S}_4\text{-T}$ (D). Copyright 2022, Elsevier, Reproduced with permission.⁹²

(E and F) Constant-current charge-discharge curves of $\text{Co}_{0.85}\text{Se}$ (E) and $\text{Co}_{0.85}\text{Se-CTAB}$ (F) at 50 mA g^{-1} .

(G) *ex situ* XRD patterns of the $\text{Co}_{0.85}\text{Se-CTAB}$ cathode under different charging and discharging states; (H) Schematic representation of the Mg storage mechanism of $\text{Co}_{0.85}\text{Se}$. Copyright 2022, Elsevier, Reproduced with permission.⁹³

(I) Schematic representation of the preparation of hollow $\text{Co}_{0.85}\text{Se/CNTs}$.

(J) TEM, HRTEM, and selected electron diffraction images of $\text{Co}_{0.85}\text{Se/CNTs}$.

(K) GCD curves of $\text{Co}_{0.85}\text{Se/CNTs}$ at 50 mA g^{-1} .

(L) Comparison of cycling performance of $\text{Co}_{0.85}\text{Se/CNT}$ and $\text{Co}_{0.85}\text{Se}$ at 50 mA g^{-1} .

(M) Long cycling performance of $\text{Co}_{0.85}\text{Se/CNT}$ and $\text{Co}_{0.85}\text{Se}$ at 200 mA g^{-1} . Copyright 2022, Elsevier, Reproduced with permission.⁹⁴

Metal-organic frameworks (MOF) are widely used as ideal precursors for the preparation of composites of metal compounds with carbon materials due to their controllable morphology and the homogeneous dispersion of metal atoms within the organic matrix.^{95–99} it is reflected in many types of batteries. For example, Xu et al.¹⁰⁰ prepared three carbon-coated metal selenides by a simple two-step calcination method using octahedral Cu-MOF, rod-shaped Fe-MOF, and hollow spherical Ni-MOF, respectively, and obtained satisfactory properties in SIBs. Hu et al.¹⁰¹ creatively grew a layer of ZIF-67 on the surface of ZIF-8, which was converted to a ZnSe-NC@CoSe-NC core-shell structure during high-temperature selenation and obtained excellent performance in SIBs and PIBs, which are sufficient to show the irreplaceable advantages of MOF as precursors. Chen and co-workers⁹⁴ also attempted to compound the carbon material with $\text{Co}_{0.85}\text{Se}$ in a unique way to enhance its properties (Figure 9I). They innovatively added carbon nanotubes (CNTs) to the cobalt salt precursor solution of ZIF-67, and after aging obtained a composite structure of carbon nanotubes interspersed in ZIF-67, which maintained the original morphology of polyhedral cages during liquid-phase salinization and transformed into hollow $\text{Co}_{0.85}\text{Se}$ penetrated by carbon nanotubes (Figure 9G). As shown in Figures 9K–9M, the $\text{Co}_{0.85}\text{Se/CNTs}$ composite in MIBs obtained a high discharge capacity close to 200 mAh g^{-1} after 20 activations at 50 mA g^{-1} and could be stably cycled for 500 cycles at 200 mA g^{-1} with a capacity retention of 76%, which was much higher than that of the $\text{Co}_{0.85}\text{Se}$ without CNTs.

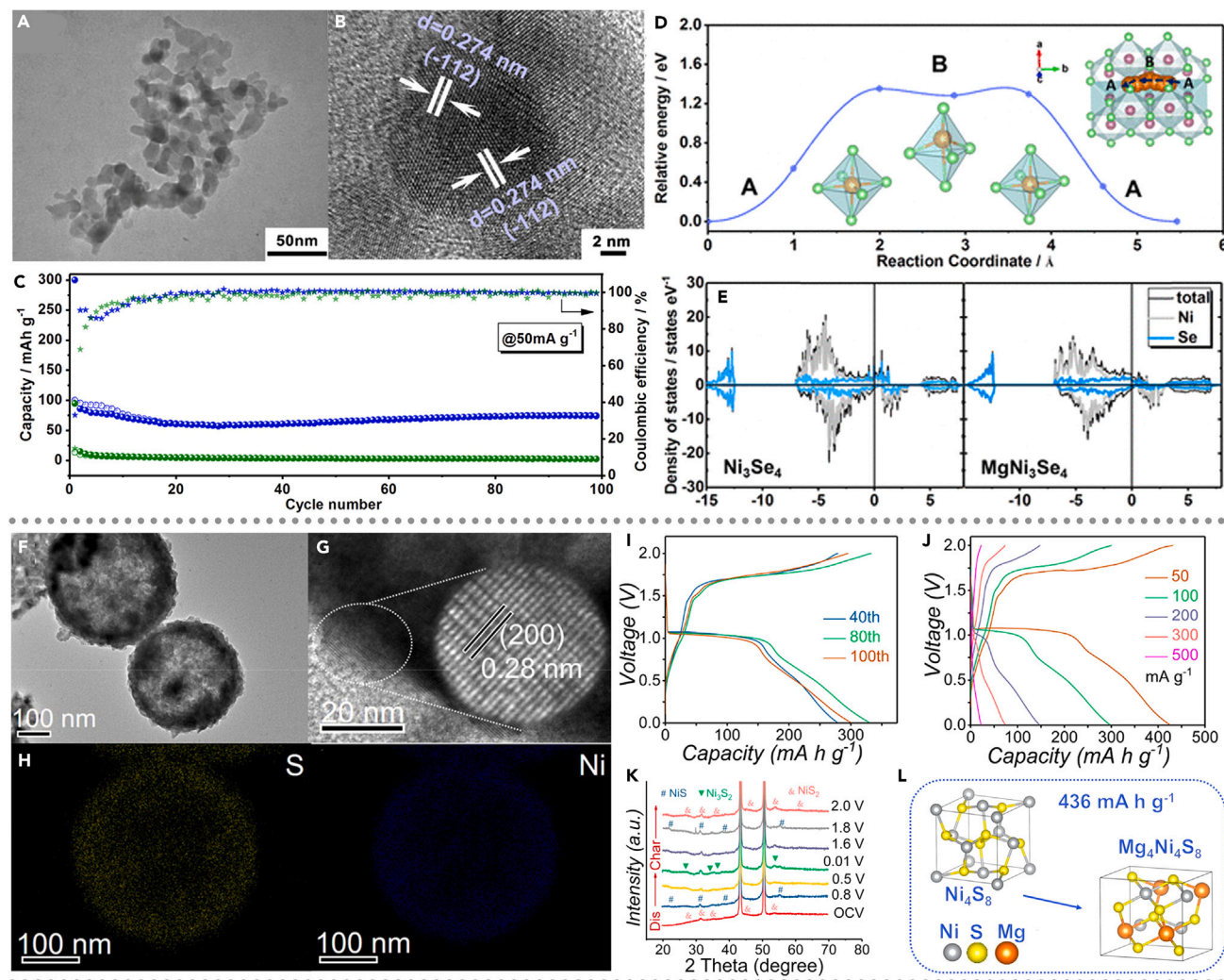


Figure 10. The application of nickel (Ni)-based sulfides cathode for MIBs

(A and B) TEM image (A), HRTEM image of Ni_3Se_4 nanoparticles (B).

(C) Comparison of cycling capacity between Ni_3Se_4 and $\text{Ni}_3\text{Se}_4\text{-Py}$.

(D) The calculated diffusion barrier and diffusion path of Mg^{2+} in Ni_3Se_4 .

(E) The total state density (TDOS) of Ni_3Se_4 and MgNi_3Se_4 . Copyright 2020, American Chemical Society, Reproduced with permission.¹⁰⁸

(F–H) TEM image (F), HRTEM image (G), EDS element mapping (H) of Ni_3Se_4 .

(I and J) GCD curves at different stages at 50 mA g^{-1} (I) and different current densities (J).

(K and L) *ex situ* XRD pattern of NiS_2 (K) and (L) Schematic diagram of DFT results. Copyright 2022, Elsevier, Reproduced with permission.¹⁰⁹

Nickel (Ni)-based sulfides

As a new generation of emerging batteries, there are relatively few reports on the cathode materials for MIBs, and a large portion of the substances that have been widely used in other fields have not been verified for their feasibility in MIBs. For example, nickel-based sulfides are known to have a wide range of applications in catalysis,^{102,103} LIBs,^{104,105} and supercapacitors (SCs),^{106,107} but there are only a few reports on nickel-based sulfides as cathode materials in MIBs, which need to be further explored and investigated by researchers. In 2020, Wei et al.¹⁰⁸ used Ni_3Se_4 as the cathode material for MIBs for the first time, which used alkaline hydrothermal method to prepare Ni_3Se_4 with a small particle size (10–20 nm) (Figures 10A and 10B). For comparison purposes, Ni_3Se_4 with a slightly larger particle size ($\text{Ni}_3\text{Se}_4\text{-Py}$) was prepared by replacing the solvent with pyridine. As shown in the Figure 10C, Ni_3Se_4 nanoparticles show a stable specific discharge capacity of 80 mA h g^{-1} at 50 mA g^{-1} , and can be stable 100 cycles. In contrast, Ni_3Se_4 ($\text{Ni}_3\text{Se}_4\text{-Py}$) has a much lower discharge capacity, only $<10 \text{ mA h g}^{-1}$. The huge difference in discharge capacity directly illustrates the great changes brought about by nanoization in MIBs electrode materials. First-principle calculations show that when Mg^{2+} is embedded in Ni_3Se_4 crystals, the diffusion energy barrier of 1.35 eV must be overcome, which results in

slow intercalation kinetics. Nanoization can greatly reduce the diffusion distance of Mg^{2+} and greatly reduce the energy required for diffusion, which is a very effective and feasible strategy (Figures 10D and 10E).

In addition, Wang et al.¹⁰⁹ used hollow spheres assembled from NiS_2 nanoparticles as cathode materials for MIBs. DFT calculation shows that the theoretical magnesium storage capacity is as high as 436 mAh g^{-1} , which has a very broad application prospect (Figure 10L). They formed a homogeneous solution of nickel acetyl acetone and TAA in ethanol, which was then cured by solvothermal reaction through Ostwald to form a particle self-assembled NiS_2 hollow sphere (Figures 10F–10S). The nanoparticles provide a large contact area with the electrolyte, while the hollow structure provides a large buffer space for the volume expansion of the material during circulation. As shown in the Figure 10I, the NiS_2 hollow sphere still exhibits up to 300 mAh g^{-1} after 100 cycles at 50 mA g^{-1} , reaching 68.8% of the theoretical capacity, which is enough to show the great advantages of its structure.

Overall, unlike the severe shuttle effect of sulfur monomers, the main reason for the slow Mg storage kinetics of transition metal sulfur compounds cathode materials are due to the strong Coulombic forces between the high charge density and the host material making the insertion/de-insertion and diffusion of Mg^{2+} into the host material exhibit sluggish and slow kinetics. This is subjectively usually manifested with the extraordinarily long activation period of MIBs, which also greatly increases the degree of difficulty in the development of MIBs. To alleviate this problem, we can often employ the synthesis of nanoscale materials with small particle sizes to reduce the total diffusion path of Mg^{2+} through the material and reduce the amount of energy required to drive Mg^{2+} . This can often be achieved using reduced solution concentrations for hydrothermal/solvent thermal. In addition to this, more advanced gas phase deposition methods can be applied to prepare small particle size transition metal sulphides. In addition to particle size reduction, the preparation of ultrathin microchip materials may also achieve such results. However, the most suitable particle size for magnesium storage materials is still vague, with no specific studies reported, and requires in-depth exploration by researchers.

SUMMARY AND OUTLOOK

In summary, we reviewed the recent reports on the application of a variety of sulfur conversion cathode materials (S, Se, Te, Cu-based and Fe-based sulfides, etc.) for MIBs cathode materials from the perspective of microstructure design. Sulfur conversion cathode materials with low preparation cost and excellent conversion capacity are considered as the key conversion cathode materials to achieve high energy density MIBs. However, the low coulombic efficiency and rapid capacity decay of chalcogenide cathode materials are usually due to their poor electrical conductivity and volume expansion caused by repeated phase conversion during cycling. In order to solve these intractable problems, researchers have made a lot of attempts from many aspects, among which the modification of microstructure is found to be a low-cost, quick effect modification strategy, the specific conclusions are as follows: (1) nanoscale; due to the strong coulombic force between Mg^{2+} and the cathode material due to the large radius of Mg^{2+} and the structural characteristics of carrying two charges, the diffusion of Mg^{2+} needs to overcome the huge diffusion energy barrier, which leads to the slow kinetics and low capacity of MIBs. By changing the experimental conditions (such as the solvent in the solvent-thermal reaction, etc.), the researchers prepared nanoparticles with small particle size, greatly reduced the diffusion path of Mg^{2+} , reduced the energy required for Mg^{2+} diffusion, and greatly improved the reaction kinetics. (2) Nanosheet self-assembly; by introducing surfactants or changing solvents in the liquid phase reaction system, the growth rate of the crystal surface can be partially inhibited, and the nanoflower morphology with a large number of folds can be obtained. Due to a large number of exposed folds, the contact between the morphology and the electrolyte becomes more fully, which greatly activates the active sites that are usually difficult to react. At the same time, because the folds are usually ultra-thin nanosheets, this has a supporting effect on the structure, and also plays a similar role to the nanoparticles, shortening the diffusion path of Mg^{2+} . (3) Atomic doping; researchers have found that the chemical properties of cations and anions are important factors to improve the electrochemical properties of converted sulfur compound cathode materials. The conductivity of raw materials can be greatly improved by anion substitution with some large volume and high polarizability cations, and the ionic diffusion barrier can be reduced by widening the lattice spacing. Among chalcogenides, Se, Te, and other elements are often used as anion doping sources due to their large volume and high conductivity, and the cathode materials replaced by ions also show satisfactory magnesium storage performance. (4) Hollow structure; researchers usually use the template method or Oswald curing to prepare the hollow structure of sulfides, hollow structure because of the huge volume cavity provides a huge buffer space for the volume expansion, can withstand the characteristics of large cycle stress, is considered to be one of the effective strategies to improve the cycle performance of electrode materials. In addition, special morphologies such as nanosheets may appear in the process of sulfuration/selenization on the surface of the template, so that the excellent morphology of the hollow cage assembled by the nanosheets can be obtained after the removal of the template. The large cavity and the morphology of the nanosheets can double regulate the function, so the nanosheets can improve the contact with the electrolyte, and the large cavity can alleviate the stress damage. (5) Composite with carbon materials; based on the previous excellent structure and a variety of conductive C materials, such as rGO, carbon nanotubes (CNTs), etc., to improve the dispersion of the nanostructure at the same time, improve the electrical conductivity of the material, accelerate the ion conduction of the material. At present, the main preparation methods of C composites include *in situ* growth, precursor derivation, carbon coating, and so on.

In short, the wide application of sulfur conversion cathode materials in MIBs and various modification strategies make it a key material to achieve high energy density. Based on the high specific capacity and cyclic stability of sulfur conversion materials, the future modification can be carried out from the following aspects: Firstly, the nanoparticles can greatly shorten the diffusion path of Mg^{2+} , but it faced serious agglomeration problems during the preparation process, which makes it difficult to obtain the desired structure. To solve this problem, researchers can try to prepare metal chalcogenides quantum dots for magnesium storage. The ultra-small size of quantum dots can greatly improve the utilization rate of electrode materials. At present, there are very few reports on magnesium storage of quantum dots.¹¹⁰ Secondly, the types of

electrolytes currently used for MIBs are too rare recently, and they are extremely sensitive to air and water, have high requirements for the battery assembly environment, and low the matching degree with the cathode material, which seriously limits the further improvement of the performance of sulfur conversion cathode materials. Thus, researchers should focus on the development of electrolytes that are highly matched with sulfides. In the development of MIBs, both electrode and electrolytes should be considered carefully. In the development of high-performance electrode materials, it is also necessary to consider the development of matching electrolytic liquid system. In addition to this, most of the MIBs cathode materials are currently prepared in small systems with stringent reactions, which greatly hinders the large-scale production and commercialization of MIBs. So, we have to shift the research focus toward the preparation method with high yield, researchers can try to prepare transition metal sulfur compounds by one-step calcination of precursors. Chitosan, PVP, etc. can be used as the precursor of carbon in the material, and by controlling the amount of metal salts and non-metal sources added, it is possible to prepare foaming porous carbon substrate loaded with transition metal sulfur compounds of composites. This preparation method not only allows easy nanosizing of the compound particles, but also provides a conductive network and rigid protection for the cycling of the compounds at the same time, which may be an optimal solution for high volume production. However, there are few relevant reports in MIBs, which are worthy of researchers' design and attempts.

Besides, if we look beyond the traditional electrode materials to the whole battery system, we will find that the Cu collector is also an important component of the energy storage of sulfur compounds, and the Cu species in the Cu collector reacts with polysulfides/polyselenides to generate copper sulfide or copper selenide into the active material, which gradually and reversibly transforms with the active material to stimulate the electrochemical performance of the electrode material. Therefore, in terms of motivation we place our research focus on the system of collector and active material. It is possible to design the surface micromorphology of Cu collector to stimulate the magnesium storage performance of sulfur compounds to a great extent.

The development of MIBs is still in the exploratory stage, and there are many challenges to be explored and solved. The current research progress shows that researchers can effectively modify the structure of chalcogenide and transition metal chalcogenides to achieve excellent magnesium storage properties.

ACKNOWLEDGMENTS

This work was supported by the National Natural Science Foundation of China (22269020, 42167068, U23A20582), Industry Support Plan Project from Gansu Provincial Department of Education (2021CYZC-09, 2023CYZC-17), 2024 Major Cultivation Project for University Research and Innovation Platforms (2024CXPT-10), Hubei Province Outstanding Youth Fund Project (2023AFA108), and the "Pioneer" and "Leading Goose" R&D Program of Zhejiang (2022SDXHDX0004).

AUTHOR CONTRIBUTIONS

W.M.: conceptualization, investigation, interpretation, compilation, visualization, and writing – original draft. H.P.: conceptualization, writing – review and editing. S.C.: writing – review and editing. J.Z.: writing – review and editing. G.M.: conceptualization, supervision, funding acquisition, and writing – review and editing. L.Z.: conceptualization, supervision, funding acquisition, and writing – review and editing. Z.L.: supervision, funding acquisition. Y.X.: conceptualization, supervision, funding acquisition, and writing – review and editing.

DECLARATION OF INTERESTS

There are no conflicts to declare.

REFERENCES

- Nematollahi, O., Hoghooghi, H., Rasti, M., and Sedaghat, A. (2016). Energy demands and renewable energy resources in the Middle East. *Renew. Sustain. Energy Rev.* 54, 1172–1181. <https://doi.org/10.1016/j.rser.2015.10.058>.
- Slameršak, A., Kallis, G., and O'Neill, D.W. (2022). Energy requirements and carbon emissions for a low-carbon energy transition. *Nat. Commun.* 13, 6932. <https://doi.org/10.1038/s41467-022-33976-5>.
- Zhao, G., Wang, X., and Negnevitsky, M. (2022). Connecting battery technologies for electric vehicles from battery materials to management. *iScience* 25, 103744. <https://doi.org/10.1016/j.isci.2022.103744>.
- El Bakkari, F., and Mounir, H. (2024). Compatible alternative energy storage systems for electric vehicles: Review of relevant technology derived from conventional systems. *Energy* 288, 129775. <https://doi.org/10.1016/j.energy.2023.129775>.
- Song, K., Agyeman, D.A., Park, M., Yang, J., and Kang, Y.M. (2017). High Energy Density Metal Oxygen Batteries: Lithium Oxygen Batteries vs Sodium Oxygen Batteries. *Adv. Mater.* 29, 1606572. <https://doi.org/10.1002/adma.201606572>.
- Durmus, Y.E., Zhang, H., Baakes, F., Desmaizieres, G., Hayun, H., Yang, L., Kolek, M., Küpers, V., Janek, J., Mandler, D., et al. (2020). Side by Side Battery Technologies with Lithium-Ion Based Batteries. *Adv. Energy Mater.* 10, 2000089. <https://doi.org/10.1002/aenm.202000089>.
- Manthiram, A. (2017). An Outlook on Lithium Ion Battery Technology. *ACS Cent. Sci.* 3, 1063–1069. <https://doi.org/10.1021/acscentsci.7b00288>.
- Li, J., Fleetwood, J., Hawley, W.B., and Kays, W. (2022). From Materials to Cell: State-of-the-Art and Prospective Technologies for Lithium-Ion Battery Electrode Processing. *Chem. Rev.* 122, 903–956. <https://doi.org/10.1021/acs.chemrev.1c00565>.
- Lu, J., Wu, T., and Amine, K. (2017). State-of-the-art characterization techniques for advanced lithium-ion batteries. *Nat. Energy* 2, 17011. <https://doi.org/10.1038/nenergy.2017.11>.
- An, J., Wang, F., Yang, J.-Y., Li, G., and Li, Y. (2024). An Ion-Pumping Interphase on Graphdiyne/Graphite Heterojunction for Fast-Charging Lithium-Ion Batteries. *CCS Chem.* 6, 110–124. <https://doi.org/10.31635/ccschem.023.202302710>.
- Vu, T.T., Cheon, H.J., Shin, S.Y., Jeong, G., Wi, E., and Chang, M. (2023). Hybrid electrolytes for solid-state lithium batteries: Challenges, progress, and prospects. *Energy Storage Mater.* 61, 102876. <https://doi.org/10.1016/j.ensm.2023.102876>.
- Ma, L., Tan, J., Wang, Y., Liu, Z., Yang, Y., Gray, T., Zhang, X., Ye, M., and Shen, J. (2023). Boron-Based High Performance Lithium Batteries: Recent Progress, Challenges, and Perspectives. *Adv. Energy*

- Mater. 13, 2300042. <https://doi.org/10.1002/aenm.202300042>.
- Rashad, M., Asif, M., Wang, Y., He, Z., and Ahmed, I. (2020). Recent advances in electrolytes and cathode materials for magnesium and hybrid-ion batteries. *Energy Storage Mater.* 25, 342–375. <https://doi.org/10.1016/j.ensm.2019.10.004>.
 - Liu, Y., Zhang, R., Wang, J., and Wang, Y. (2021). Current and future lithium-ion battery manufacturing. *iScience* 24, 102332. <https://doi.org/10.1016/j.isci.2021.102332>.
 - Fan, X., Tebyetekerwa, M., Wu, Y., Gaddam, R.R., and Zhao, X.S. (2022). Origin of Excellent Charge Storage Properties of Defective Tin Disulphide in Magnesium/Lithium-Ion Hybrid Batteries. *Nano-Micro Lett.* 14, 177. <https://doi.org/10.1007/s40820-022-00914-5>.
 - Das, A., Balakrishnan, N.T., Sreeram, P., Fatima, M.J., Joyner, J.D., Thakur, V.K., Pullanchiyodan, A., Ahn, J.H., and Raghavan, P. (2024). Prospects for magnesium ion batteries: A comprehensive materials review. *Coord. Chem. Rev.* 502, 215593. <https://doi.org/10.1016/j.ccr.2023.215593>.
 - Guo, Q., Zeng, W., Liu, S.-L., Li, Y.-Q., Xu, J.-Y., Wang, J.-X., and Wang, Y. (2020). Recent developments on anode materials for magnesium-ion batteries: a review. *Rare Met.* 40, 290–308. <https://doi.org/10.1007/s12598-020-01493-3>.
 - Wei, C., Tan, L., Zhang, Y., Wang, Z., Feng, J., and Qian, Y. (2022). Towards better Mg metal anodes in rechargeable Mg batteries: Challenges, strategies, and perspectives. *Energy Storage Mater.* 52, 299–319. <https://doi.org/10.1016/j.ensm.2022.08.014>.
 - Gabriel, E., Ma, C., Graff, K., Conrado, A., Hou, D., and Xiong, H. (2023). Heterostructure engineering in electrode materials for sodium-ion batteries: Recent progress and perspectives. *eScience* 3, 100139. <https://doi.org/10.1016/j.esci.2023.100139>.
 - Niu, J., Zhang, Z., and Aurbach, D. (2020). Alloy Anode Materials for Rechargeable Mg Ion Batteries. *Adv. Energy Mater.* 10, 2000697. <https://doi.org/10.1002/aenm.202000697>.
 - Ge, X., Song, F., Du, A., Zhang, Y., Xie, B., Huang, L., Zhao, J., Dong, S., Zhou, X., and Cui, G. (2022). Robust Self-Standing Single-Ion Polymer Electrolytes Enabling High-Safety Magnesium Batteries at Elevated Temperature. *Adv. Energy Mater.* 12, 2201464. <https://doi.org/10.1002/aenm.202201464>.
 - Gao, Y., Pan, Z., Sun, J., Liu, Z., and Wang, J. (2022). High-Energy Batteries: Beyond Lithium-Ion and Their Long Road to Commercialisation. *Nano-Micro Lett.* 14, 94. <https://doi.org/10.1007/s40820-022-00844-2>.
 - Tan, S., Xiong, F., Wang, J., An, Q., and Mai, L. (2020). Crystal regulation towards rechargeable magnesium battery cathode materials. *Mater. Horiz.* 7, 1971–1995. <https://doi.org/10.1039/d0mh00315h>.
 - Ng, K.L., Shu, K., and Azimi, G. (2022). A rechargeable Mg|O₂ battery. *iScience* 25, 104711. <https://doi.org/10.1016/j.isci.2022.104711>.
 - Liu, B., Zhang, Q., Li, Y., Hao, Y., Ali, U., Li, L., Zhang, L., Wang, C., and Su, Z. (2023). Realizing Complete Solid-Solution Reaction to Achieve Temperature Independent LiFePO₄ for High Rate and Low Temperature Li-Ion Batteries. *CCS Chem.* 5, 209–220. <https://doi.org/10.31635/ccschem.022.202201776>.
 - Zhang, Z., Cui, Z., Qiao, L., Guan, J., Xu, H., Wang, X., Hu, P., Du, H., Li, S., Zhou, X., et al. (2017). Novel Design Concepts of Efficient Mg-Ion Electrolytes toward High-Performance Magnesium–Selenium and Magnesium–Sulfur Batteries. *Adv. Energy Mater.* 7, 1602055. <https://doi.org/10.1002/aenm.201602055>.
 - Song, M., Niu, J., Yin, K., Gao, H., Zhang, C., Ma, W., Luo, F., Peng, Z., and Zhang, Z. (2019). Self-supporting, eutectic-like, nanoporous biphasic bismuth-tin film for high-performance magnesium storage. *Nano Res.* 12, 801–808. <https://doi.org/10.1007/s12274-019-2291-1>.
 - Wang, Y., Yang, X., Zhang, Z., Hu, X., Meng, Y., Wang, X., Zhou, D., Liu, H., Li, B., and Wang, G. (2022). Electrolyte design for rechargeable anion shuttle batteries. *eScience* 2, 573–590. <https://doi.org/10.1016/j.esci.2022.10.003>.
 - Lossius, L.P., and Emmenegger, F. (1996). Plating of magnesium from organic solvents. *Electrochim. Acta* 41, 445–447. [https://doi.org/10.1016/0013-4686\(95\)00326-6](https://doi.org/10.1016/0013-4686(95)00326-6).
 - Xue, X., Song, X., Tao, A., Yan, W., Zhang, X.L., Tie, Z., and Jin, Z. (2022). Boosting the cycling stability of rechargeable magnesium batteries by regulating the compatibility between nanostructural metal sulfide cathodes and non-nucleophilic electrolytes. *Nano Res.* 16, 2399–2408. <https://doi.org/10.1007/s12274-022-4932-z>.
 - Zhen, J., Shen, J., Sun, T., Wang, C., Lyu, P., and Xu, Y. (2024). Direct Synthesis of Ultrathin Crystalline Two-Dimensional Triazine Polymers from Aldoximes. *CCS Chem.* 6, 932–940. <https://doi.org/10.31635/ccschem.023.202303111>.
 - Man, Y., Jaumaux, P., Xu, Y., Fei, Y., Mo, X., Wang, G., and Zhou, X. (2023). Research development on electrolytes for magnesium-ion batteries. *Sci. Bull.* 68, 1819–1842. <https://doi.org/10.1016/j.scib.2023.07.027>.
 - Li, C., Lin, L., Wu, W., and Sun, X. (2022). A High Potential Polyanion Cathode Material for Rechargeable Mg-Ion Batteries. *Small Methods* 6, 2200363. <https://doi.org/10.1002/smtd.202200363>.
 - Huie, M.M., Bock, D.C., Takeuchi, E.S., Marschilok, A.C., and Takeuchi, K.J. (2015). Cathode materials for magnesium and magnesium-ion based batteries. *Coord. Chem. Rev.* 287, 15–27. <https://doi.org/10.1016/j.ccr.2014.11.005>.
 - He, X., Cheng, R., Sun, X., Xu, H., Li, Z., Sun, F., Zhan, Y., Zou, J., and Laine, R.M. (2023). Organic cathode materials for rechargeable magnesium-ion batteries: Fundamentals, recent advances, and approaches to optimization. *J. Magnes. Alloy.* 11, 4359–4389. <https://doi.org/10.1016/j.jma.2023.11.008>.
 - Shi, M., Li, T., Shang, H., Zhang, D., Qi, H., Huang, T., Xie, Z., Qi, J., Wei, F., Meng, Q., et al. (2023). A critical review of inorganic cathode materials for rechargeable magnesium ion batteries. *J. Energy Storage* 68, 107765. <https://doi.org/10.1016/j.est.2023.107765>.
 - Aurbach, D., Lu, Z., Schechter, A., Gofer, Y., Gizbar, H., Turgeman, R., Cohen, Y., Moshkovich, M., and Levi, E. (2000). Prototype systems for rechargeable magnesium batteries. *Nature* 407, 724–727. <https://doi.org/10.1038/35037553>.
 - Yao, Y.Y., Zhan, Y., Sun, X.Y., Li, Z., Xu, H., Laine, R.M., and Zou, J.X. (2023). Advances in Cathodes for High-Performance Magnesium-Sulfur Batteries: A Critical Review. *Batteries* 9, 203. <https://doi.org/10.3390/batteries9040203>.
 - Liu, F., Wang, T., Liu, X., and Fan, L.Z. (2020). Challenges and Recent Progress on Key Materials for Rechargeable Magnesium Batteries. *Adv. Energy Mater.* 11, 2000787. <https://doi.org/10.1002/aenm.202000787>.
 - Yuan, J., Yu, B., Pan, D., Hu, X., Chen, J., Aminua, M., Liu, Y., Sheng, L., Chen, Y., Wu, Y., et al. (2023). Universal Source-Template Route to Metal Selenides Implanting on 3D Carbon Nanoarchitecture: Cu₂-xSe@3D-CN with Se-C Bonding for Advanced Na Storage. *Adv. Funct. Mater.* 33, 2305503. <https://doi.org/10.1002/adfm.202305503>.
 - Kotobuki, M., Yan, B., and Lu, L. (2023). Recent progress on cathode materials for rechargeable magnesium batteries. *Energy Storage Mater.* 54, 227–253. <https://doi.org/10.1016/j.ensm.2022.10.034>.
 - Mao, M., Gao, T., Hou, S., and Wang, C. (2018). A critical review of cathodes for rechargeable Mg batteries. *Chem. Soc. Rev.* 47, 8804–8841. <https://doi.org/10.1039/c8cs00319j>.
 - Cabello, M., Medina, A., Alcántara, R., Nacimiento, F., Pérez-Vicente, C., and Tirado, J.L. (2020). A theoretical and experimental study of hexagonal molybdenum trioxide as dual-ion electrode for rechargeable magnesium battery. *J. Alloys Compd.* 831, 154795. <https://doi.org/10.1016/j.jallcom.2020.154795>.
 - Perera, S.D., Archer, R.B., Damin, C.A., Mendoza-Cruz, R., and Rhodes, C.P. (2017). Controlling interlayer interactions in vanadium pentoxide-poly(ethylene oxide) nanocomposites for enhanced magnesium-ion charge transport and storage. *J. Power Sources* 343, 580–591. <https://doi.org/10.1016/j.jpowsour.2017.01.052>.
 - Pan, J., Wang, X., Li, H., Cui, Z., Chen, H., Nie, J., Gou, H., Yu, D., Chen, C., and Liu, Y. (2022). The Conversion-Type Selenides as Potential High-Energy Cathode Materials for Mg-Based Batteries: A Review. *ACS Sustain. Chem. Eng.* 10, 14980–15006. <https://doi.org/10.1021/acssuschemeng.2c05222>.
 - Zhang, Z., Dong, S., Cui, Z., Du, A., Li, G., and Cui, G. (2018). Rechargeable Magnesium Batteries using Conversion-Type Cathodes: A Perspective and Minireview. *Small Methods* 2, 1800020. <https://doi.org/10.1002/smtd.201800020>.
 - Wang, S., and Zhao, X. (2023). Minireview on Metal–Chalcogenide Cathode Materials with Dual-Redox Centers for Magnesium–Metal-Anode-Based Batteries: Recent Progress and Future Directions. *Energy Fuels* 37, 18441–18455. <https://doi.org/10.1021/acs.energyfuels.3c03057>.
 - Yu, T., Li, G., Duan, Y., Wu, Y., Zhang, T., Zhao, X., Luo, M., and Liu, Y. (2023). The research and industrialization progress and prospects of sodium ion battery. *J. Alloys Compd.* 958, 170486. <https://doi.org/10.1016/j.jallcom.2023.170486>.
 - Nguyen, D.-T., Horia, R., Eng, A.Y.S., Song, S.-W., and Seh, Z.W. (2021). Material design strategies to improve the performance of rechargeable magnesium–sulfur batteries.

- Mater. Horiz. 8, 830–853. <https://doi.org/10.1039/d0mh01403f>.
50. Regulacio, M.D., Nguyen, D.T., Horia, R., and Seh, Z.W. (2021). Designing Nanostructured Metal Chalcogenides as Cathode Materials for Rechargeable Magnesium Batteries. *Small* 17, 2007683. <https://doi.org/10.1002/sml.202007683>.
 51. Wang, Z., Zhu, Y., Peng, H., Du, C., Ma, X., and Cao, C. (2021). Microwave-induced phase engineering of copper sulfide nanosheets for rechargeable magnesium batteries. *Electrochim. Acta* 374, 137965. <https://doi.org/10.1016/j.electacta.2021.137965>.
 52. Blanc, L.E., Sun, X., Shyamsunder, A., Duffort, V., and Nazar, L.F. (2020). Direct Nano-Synthesis Methods Notably Benefit Mg-Battery Cathode Performance. *Small Methods* 4, 2000029. <https://doi.org/10.1002/smt.202000029>.
 53. Xu, R., Wei, R., Hu, X., Li, Y., Wang, L., Zhang, K., Wang, Y., Zhang, H., Liang, F., and Yao, Y. (2021). A strategy and detailed explanations to the composites of Si/MWCNTs for lithium storage. *Carbon* 171, 265–275. <https://doi.org/10.1016/j.carbon.2020.08.073>.
 54. Wang, W., Yuan, H., NuLi, Y., Zhou, J., Yang, J., and Wang, J. (2018). Sulfur@microporous Carbon Cathode with a High Sulfur Content for Magnesium–Sulfur Batteries with Nucleophilic Electrolytes. *J. Phys. Chem. C* 122, 26764–26776. <https://doi.org/10.1021/acs.jpcc.8b09003>.
 55. Chen, Z., Yang, Q., Wang, D., Chen, A., Li, X., Huang, Z., Liang, G., Wang, Y., and Zhi, C. (2022). Tellurium: A High-Performance Cathode for Magnesium Ion Batteries Based on a Conversion Mechanism. *ACS Nano* 16, 5349–5357. <https://doi.org/10.1021/acsnano.1c07939>.
 56. Zhang, Y., Li, X., Shen, J., Chen, Z., Cao, S.-a., Li, T., and Xu, F. (2019). Rechargeable Mg batteries based on a Ag₂S conversion cathode with fast solid-state Mg²⁺ diffusion kinetics. *Dalton T* 48, 14390–14397. <https://doi.org/10.1039/c9dt02221j>.
 57. Liu, F., Wang, T., Liu, X., Jiang, N., and Fan, L.-Z. (2021). High-performance heterojunction Ti₃C₂/CoSe₂ with both intercalation and conversion storage mechanisms for magnesium batteries. *Chem. Eng. J.* 426, 130747. <https://doi.org/10.1016/j.cej.2021.130747>.
 58. Shen, Y., Wang, Y., Miao, Y., Yang, M., Zhao, X., and Shen, X. (2020). High-Energy Interlayer-Expanded Copper Sulfide Cathode Material in Non-Corrosive Electrolyte for Rechargeable Magnesium Batteries. *Adv. Mater.* 32, 1905524. <https://doi.org/10.1002/adma.201905524>.
 59. Chen, D., Zhang, Y., Li, X., Shen, J., Chen, Z., Cao, S.-a., Li, T., and Xu, F. (2020). Nanosheets assembling hierarchical starfish-like Cu_{2-x}Se as advanced cathode for rechargeable Mg batteries. *Chem. Eng. J.* 384, 123235. <https://doi.org/10.1016/j.cej.2019.123235>.
 60. Zhao, W., Zhang, Y., Li, H., Shen, Y., Wang, K., and Jiang, K. (2023). Non-stoichiometric Cu_{2-x}Se hollow nanocubes cathodes enabling high-rate capability and ultra-long cyclic stability rechargeable Mg batteries. *Chem. Eng. J.* 464, 142654. <https://doi.org/10.1016/j.cej.2023.142654>.
 61. Yang, X., Du, C., Zhu, Y., Peng, H., Liu, B., Cao, Y., Zhang, Y., Ma, X., and Cao, C. (2022). Constructing defect-rich unconventional phase Cu₇2S₄ nanotubes via microwave-induced selective etching for ultra-stable rechargeable magnesium batteries. *Chem. Eng. J.* 430, 133108. <https://doi.org/10.1016/j.cej.2021.133108>.
 62. Zhu, G., Wang, W., and Yu, X. (2022). Benzoate anion derived carbon-encapsulated NiS nanoparticles as a freestanding cathode for magnesium-based batteries. *J. Alloys Compd.* 919, 165835. <https://doi.org/10.1016/j.jallcom.2022.165835>.
 63. Mao, M., Tong, Y., Zhang, Q., Hu, Y.-S., Li, H., Huang, X., Chen, L., Gu, L., and Suo, L. (2020). Joint Cationic and Anionic Redox Chemistry for Advanced Mg Batteries. *Nano Lett.* 20, 6852–6858. <https://doi.org/10.1021/acs.nanolett.0c02908>.
 64. Wang, Z., Chen, S., Wang, L., Gao, S., Li, M., Li, H., Zhu, Y., and Shangguang, E. (2023). Microwave-anion-exchange route to spinel CuCo₂S₄ nanosheets as cathode materials for magnesium storage. *J. Power Sources* 556, 232480. <https://doi.org/10.1016/j.jpowsour.2022.232480>.
 65. Du, C., Han, Z., Peng, H., Tian, J., Yang, X., Xia, T., Ma, X., Zhu, Y., and Cao, C. (2022). Kinetically optimized copper sulfide cathodes for rechargeable magnesium batteries. *J. Power Sources* 546, 231673. <https://doi.org/10.1016/j.jpowsour.2022.231673>.
 66. Shen, Y., Zhang, Q., Wang, Y., Gu, L., Zhao, X., and Shen, X. (2021). A Pyrite Iron Disulfide Cathode with a Copper Current Collector for High-Energy Reversible Magnesium-Ion Storage. *Adv. Mater.* 33, 2103881. <https://doi.org/10.1002/adma.202103881>.
 67. Liu, T., Hu, H., Ding, X., Yuan, H., Jin, C., Nai, J., Liu, Y., Wang, Y., Wan, Y., and Tao, X. (2020). 12 years roadmap of the sulfur cathode for lithium sulfur batteries (2009–2020). *Energy Storage Mater.* 30, 346–366. <https://doi.org/10.1016/j.ensm.2020.05.023>.
 68. Lu, Y., Wang, C., Liu, Q., Li, X., Zhao, X., and Guo, Z. (2021). Progress and Perspective on Rechargeable Magnesium–Sulfur Batteries. *Small Methods* 5, 2001303. <https://doi.org/10.1002/smt.202001303>.
 69. Montenegro, C.T., Peters, J.F., Baumann, M., Zhao-Karger, Z., Wolter, C., and Weil, M. (2021). Environmental assessment of a new generation battery: The magnesium-sulfur system. *J. Energy Storage* 35, 102053. <https://doi.org/10.1016/j.est.2020.102053>.
 70. Wang, P., and Buchmeiser, M.R. (2019). Rechargeable Magnesium–Sulfur Battery Technology: State of the Art and Key Challenges. *Adv. Funct. Mater.* 29, 1905248. <https://doi.org/10.1002/adfm.201905248>.
 71. Liu, X., Li, Y., Xu, X., Zhou, L., and Mai, L. (2021). Rechargeable metal (Li, Na, Mg, Al)-sulfur batteries: Materials and advances. *J. Energy Chem.* 61, 104–134. <https://doi.org/10.1016/j.jechem.2021.02.028>.
 72. Laskowski, F.A.L., Stradley, S.H., Qian, M.D., and See, K.A. (2021). Mg Anode Passivation Caused by the Reaction of Dissolved Sulfur in Mg–S Batteries. *ACS Appl. Mater. Interfaces* 13, 29461–29470. <https://doi.org/10.1021/acsaami.1c02788>.
 73. Li, Z., Welle, A., Vincent, S., Wang, L., Fuchs, S., Riedel, S., Roy, A., Bosubabu, D., García-Lastra, J.M., Fichtner, M., and Zhao-Karger, Z. (2023). Addressing the Sluggish Kinetics of Sulfur Redox for High-Energy Mg–S Batteries. *Adv. Energy Mater.* 13, 2302905. <https://doi.org/10.1002/aenm.202302905>.
 74. Vinayan, B.P., Zhao-Karger, Z., Diemant, T., Chakravadhanula, V.S.K., Schwarzbürger, N.I., Cambaz, M.A., Behm, R.J., Kübel, C., and Fichtner, M. (2016). Performance study of magnesium–sulfur battery using a graphene based sulfur composite cathode electrode and a non-nucleophilic Mg electrolyte. *Nanoscale* 8, 3296–3306. <https://doi.org/10.1039/c5nr04383b>.
 75. Yu, X., and Manthiram, A. (2016). Performance Enhancement and Mechanistic Studies of Magnesium–Sulfur Cells with an Advanced Cathode Structure. *ACS Energy Lett.* 1, 431–437. <https://doi.org/10.1021/acsenergylett.6b00213>.
 76. Wu, D., Ren, W., Yang, Y., Wang, J., and NuLi, Y. (2021). A Se-Doped S@CMK3 Composite as a High-Performance Cathode for Magnesium–Sulfur Batteries with Mg²⁺/Li⁺ Hybrid Electrolytes. *J. Phys. Chem. C* 125, 25959–25967. <https://doi.org/10.1021/acs.jpcc.1c07324>.
 77. Zhao-Karger, Z., Lin, X.-M., Bonatto Minella, C., Wang, D., Diemant, T., Behm, R.J., and Fichtner, M. (2016). Selenium and selenium-sulfur cathode materials for high-energy rechargeable magnesium batteries. *J. Power Sources* 323, 213–219. <https://doi.org/10.1016/j.jpowsour.2016.05.034>.
 78. Liu, X., Zhang, Q., Du, C., Du, X., Zhu, Y., and Cao, C. (2023). Current material design strategies on the copper chalcogenide cathodes for rechargeable magnesium batteries: a review. *Mater. Chem. Front.* 7, 4400–4419. <https://doi.org/10.1039/d3qm00366c>.
 79. Duffort, V., Sun, X., and Nazar, L.F. (2016). Screening for positive electrodes for magnesium batteries: a protocol for studies at elevated temperatures. *Chem. Commun.* 52, 12458–12461. <https://doi.org/10.1039/c6cc05363g>.
 80. Wu, M., Zhang, Y., Li, T., Chen, Z., Cao, S.-a., and Xu, F. (2018). Copper sulfide nanoparticles as high-performance cathode materials for magnesium secondary batteries. *Nanoscale* 10, 12526–12534. <https://doi.org/10.1039/c8nr03375g>.
 81. Zhang, Q., Hu, Y., Wang, J., and Pan, F. (2023). Low-temperature synthesis of CuS nanospheres as cathode material for magnesium second batteries. *J. Magnes. Alloy.* 11, 192–200. <https://doi.org/10.1016/j.jjma.2021.05.017>.
 82. Huang, J., Zhu, Y., Du, C., Han, Z., Yao, X., Yang, X., Cao, Y., Zhang, Y., Ma, X., and Cao, C. (2021). Hierarchical nanosheet-assembled copper sulfide microspheres as the cathode materials for rechargeable magnesium batteries. *Electrochim. Acta* 388, 138619. <https://doi.org/10.1016/j.electacta.2021.138619>.
 83. Zhang, Y., Zhu, Y., Wang, Z., Peng, H., Yang, X., Cao, Y., Du, C., Ma, X., and Cao, C. (2021). Pulverization-Tolerant CuSe Nanoflakes with High (110) Planar Orientation for High-Performance Magnesium Storage. *Adv. Funct. Mater.* 31, 2104730. <https://doi.org/10.1002/adfm.202104730>.
 84. Shen, J., Zhang, Y., Chen, D., Li, X., Chen, Z., Cao, S.-a., Li, T., and Xu, F. (2019). A hollow CuS nanocube cathode for rechargeable Mg batteries: effect of the structure on the performance. *J. Mater. Chem. A* 7, 21410–21420. <https://doi.org/10.1039/c9ta07470h>.

85. Du, C., Younas, W., Wang, Z., Yang, X., Meng, E., Wang, L., Huang, J., Ma, X., Zhu, Y., and Cao, C. (2021). Constructing sheet-assembled hollow CuSe nanocubes to boost the rate capability of rechargeable magnesium batteries. *J. Mater. Chem. A* 9, 3648–3656. <https://doi.org/10.1039/d0ta10708e>.
86. Cao, Y., Zhu, Y., Du, C., Yang, X., Xia, T., Ma, X., and Cao, C. (2022). Anionic Te-Substitution Boosting the Reversible Redox in CuS Nanosheet Cathodes for Magnesium Storage. *ACS Nano* 16, 1578–1588. <https://doi.org/10.1021/acsnano.1c10253>.
87. Du, C., Zhu, Y., Yang, X., Lv, Z., Tian, J., Pei, X., Liu, X., Ma, X., Hou, J., and Cao, C. (2023). Lattice expanding by Te-substitution to boost electrochemical Mg storage of Cu₇.254 nanotube cathode. *Chem. Eng. J.* 458, 141345. <https://doi.org/10.1016/j.cej.2023.141345>.
88. Liu, X., Zhu, Y., Du, C., Tian, J., Yang, L., Yao, X., Wang, Z., Ma, X., Hou, J., and Cao, C. (2023). Cationic Co-doping in copper sulfide nanosheet cathodes for efficient magnesium storage. *Chem. Eng. J.* 463, 142433. <https://doi.org/10.1016/j.cej.2023.142433>.
89. Xu, H., Li, Y., Zhu, D., Li, Z., Sun, F., Zhu, W., Chen, Y., Zhang, J., Ren, L., Zhang, S., et al. (2022). Synchrotron Radiation Spectroscopic Studies of Mg²⁺ Storage Mechanisms in High-Performance Rechargeable Magnesium Batteries with Co-Doped FeS₂ Cathodes. *Adv. Energy Mater.* 12, 2201608. <https://doi.org/10.1002/aenm.202201608>.
90. Shen, Y., Wang, Y., Miao, Y., Li, Q., Zhao, X., and Shen, X. (2023). Anion-Incorporated Mg-Ion Solvation Modulation Enables Fast Magnesium Storage Kinetics of Conversion-Type Cathode Materials. *Adv. Mater.* 35, 2208289. <https://doi.org/10.1002/adma.202208289>.
91. Wang, J., Yang, G., Ghosh, T., Bai, Y., Lim, C.Y.J., Zhang, L., Seng, D.H.L., Goh, W.P., Xing, Z., Liu, Z., and Seh, Z.W. (2024). Hierarchical FeS₂ cathode with suppressed shuttle effect for high performance magnesium-ion batteries. *Nano Energy* 119, 109082. <https://doi.org/10.1016/j.nanoen.2023.109082>.
92. Cai, X., Yu, L., Dong, J., Cen, Y., Zhu, T., Yu, D., Chen, C., Zhang, D., Liu, Y., and Pan, F. (2022). Revealing the electrochemical mechanism of the conversion-type Co₃S₄ in a novel high-capacity Mg-Li hybrid battery. *Electrochim. Acta* 401, 139403. <https://doi.org/10.1016/j.electacta.2021.139403>.
93. Gao, Z., Zhang, J., Mu, T., Zhu, Y., Liu, Y., and Li, L. (2022). CTAB-assisted one-pot hydrothermal synthesis of Co_{0.85}Se as a promising cathode material for magnesium ion battery. *Mater. Lett.* 328, 133066. <https://doi.org/10.1016/j.matlet.2022.133066>.
94. Chen, D., Du, F., Cao, S.-a., Li, T., and Xu, F. (2022). Co_{0.85}Se hollow polyhedrons entangled by carbon nanotubes as a high-performance cathode for magnesium secondary batteries. *Chem. Eng. J.* 428, 129545. <https://doi.org/10.1016/j.cej.2021.129545>.
95. Shen, M., and Ma, H. (2022). Metal-organic frameworks (MOFs) and their derivative as electrode materials for lithium-ion batteries. *Coord. Chem. Rev.* 470, 214715. <https://doi.org/10.1016/j.ccr.2022.214715>.
96. Du, W., Bai, Y.-L., Xu, J., Zhao, H., Zhang, L., Li, X., and Zhang, J. (2018). Advanced metal-organic frameworks (MOFs) and their derived electrode materials for supercapacitors. *J. Power Sources* 402, 281–295. <https://doi.org/10.1016/j.jpowsour.2018.09.023>.
97. Zhao, R., Liang, Z., Zou, R., and Xu, Q. (2018). Metal-Organic Frameworks for Batteries. *Joule* 2, 2235–2259. <https://doi.org/10.1016/j.joule.2018.09.019>.
98. Song, G., Shi, Y., Jiang, S., and Pang, H. (2023). Recent Progress in MOF-Derived Porous Materials as Electrodes for High-Performance Lithium-Ion Batteries. *Adv. Funct. Mater.* 33, 2303121. <https://doi.org/10.1002/adfm.202303121>.
99. Wang, X., Zhang, G., Yin, W., Zheng, S., Kong, Q., Tian, J., and Pang, H. (2022). Metal-organic framework-derived phosphide nanomaterials for electrochemical applications. *Carbon Energy* 4, 246–281. <https://doi.org/10.1002/cey2.182>.
100. Xu, X., Liu, J., Liu, J., Ouyang, L., Hu, R., Wang, H., Yang, L., and Zhu, M. (2018). A General Metal-Organic Framework (MOF)-Derived Selenidation Strategy for In Situ Carbon-Encapsulated Metal Selenides as High-Rate Anodes for Na-Ion Batteries. *Adv. Funct. Mater.* 28, 1707573. <https://doi.org/10.1002/adfm.201707573>.
101. Hu, X., Liu, X., Chen, K., Wang, G., and Wang, H. (2019). Core-shell MOF-derived N-doped yolk-shell carbon nanocages homogeneously filled with ZnSe and CoSe₂ nanodots as excellent anode materials for lithium- and sodium-ion batteries. *J. Mater. Chem. A* 7, 11016–11037. <https://doi.org/10.1039/c9ta01999e>.
102. Lynch, B.B., Kelliher, A.P., Anderson, B.D., Japit, A., Spencer, M.A., Rizvi, M.H., Sarac, M.F., Augustyn, V., and Tracy, J.B. (2020). Sulfidation and selenidation of nickel nanoparticles. *Carbon Energy* 3, 582–589. <https://doi.org/10.1002/cey2.83>.
103. Han, S., Hao, Y., Guo, Z., Yu, D., Huang, H., Hu, F., Li, L., Chen, H.-Y., and Peng, S. (2020). Self-supported N-doped NiSe₂ hierarchical porous nanoflake arrays for efficient oxygen electrocatalysis in flexible zinc-air batteries. *Chem. Eng. J.* 401, 126088. <https://doi.org/10.1016/j.cej.2020.126088>.
104. Hu, J., Wang, H., Xiao, B., Liu, P., Huang, T., Li, Y., Ren, X., Zhang, Q., Liu, J., Ouyang, X., and Sun, X. (2023). Challenges and approaches of single-crystal Ni-rich layered cathodes in lithium batteries. *Natl. Sci. Rev.* 10, nwad252. <https://doi.org/10.1093/nsr/nwad252>.
105. Guo, H.J., Sun, Y., Zhao, Y., Liu, G.X., Song, Y.X., Wan, J., Jiang, K.C., Guo, Y.G., Sun, X., and Wen, R. (2022). Surface Degradation of Single-crystalline Ni-rich Cathode and Regulation Mechanism by Atomic Layer Deposition in Solid-State Lithium Batteries. *Angew. Chem. Int. Ed. Engl.* 61, e202211626. <https://doi.org/10.1002/anie.202211626>.
106. Zhang, L., Shi, D., Liu, T., Jaroniec, M., and Yu, J. (2019). Nickel-based materials for supercapacitors. *Mater. Today* 25, 35–65. <https://doi.org/10.1016/j.mattod.2018.11.002>.
107. Li, Y., Zhang, J., Chen, Z., and Chen, M. (2022). Nickel-based materials: Toward practical application of the aqueous hybrid supercapacitors. *Sustain. Mater. Technol.* 33, e00479. <https://doi.org/10.1016/j.susmat.2022.e00479>.
108. Wei, L., Lian, R., Zhao, Y., Meng, Y., He, L., Yu, Y., Chen, G., and Wei, Y. (2020). Experimental Investigation and First-Principles Calculations of a Ni₃Se₄ Cathode Material for Mg-Ion Batteries. *ACS Appl. Mater. Interfaces* 12, 9316–9321. <https://doi.org/10.1021/acsami.9b21540>.
109. Wang, J., Handoko, A.D., Bai, Y., Yang, G., Li, Y., Xing, Z., Ng, M.-F., and Seh, Z.W. (2022). High-Performance NiS₂ Hollow Nanosphere Cathodes in Magnesium-Ion Batteries Enabled by Tunable Redox Chemistry. *Nano Lett.* 22, 10184–10191. <https://doi.org/10.1021/acs.nanolett.2c04293>.
110. Fei, Y., Man, Y., Sun, J., Du, Y., Chen, B., Bao, J., and Zhou, X. (2023). Implanting CuS Quantum Dots into Carbon Nanorods for Efficient Magnesium Ion Batteries. *Small* 19, 2301954. <https://doi.org/10.1002/sml.202301954>.